ELECTRICAL CAPACITANCE AND RESISTANCE TOMOGRAPHY WITH VOLTAGE EXCITATION

A THESIS SUBMITTED TO THE UNIVERSITY OF MANCHESTER
FOR THE DEGREE OF MASTER OF PHILOSOPHY
IN THE FACULTY OF ENGINEERING AND PHYSICAL SCIENCES

2015

By
Marco Antonio Rodriguez Frias
Candidate
School of Electrical and Electronic Engineering

Contents

List of Tables

List of Figures

Abstract

Multi-phase flow measurement is a challenging task due to the involvement of different flow regimes, materials and a varying water-in-liquid ratio (WLR). One approach researchers have taken to tackle this difficult task, is the development of dual-modality imaging systems, fusing Electrical Capacitance Tomography (ECT) and Electrical Resistance Tomography (ERT) in a single measuring device. This is due to the ability of each technique to take advantage of different phenomena, i.e. imaging conductive media is a demanding task for ECT, but ERT yields good quality results. On the other hand, with an ERT system is not possible to get any information regarding the region of interest if there is no conductive media to allow the current to flow, but in this case ECT can perform the imaging exploiting the materials' dielectric properties. Because of those characteristics dual-modality tomography has been foreseen as a practical and a low cost solution to image a wide range of complex media.

Through years, ERT has proven to be an effective and a low cost imaging technique, but in order to integrate it to a dual-modality imaging system in parallel with ECT, it is necessary to improve it and at the same time to make it more compatible to the capacitive imaging technique, allowing in this way to exploit the best capabilities of both modalities. This requires a complete sensor and circuitry redesign.

An ERT system has been developed featuring a voltage excitation and current measurement sensing scheme making use of an ECT sensor built with electrodes inside the vessel and an available data acquisition system. This set up images successfully non-conductive material over liquid solutions with low and high conductivities as a background.

A comparison between current excitation and voltage measurement ERT and voltage excitation and current measurement ERT is performed showing that the latter not only makes ERT more suitable to integrate with a ECT system, but also improves its performance. The design of a sensor with internal electrodes and driven external guards can reduce notably the fringe effect and improve the images obtained by means of an ERT system.

8

Declaration

No portion of the work referred to in this thesis has been submitted in support of an application for another degree or qualification of this or any other university or other institute of learning.

Copyright

Acknowledgements

To my parents that have given me their love, support and their example. To my sisters and nieces for years of love, learning and support. To the rest of my lovely family.

To CONACYT, for supporting this studies.

To my supervisor, Professor Wuqiang Yang for his patience and his wise guidance throughout my studies.

To Michelle, for her company and Luis for his friendship.

To Mexico.

Agradecimientos

A mis padres que me han dado su amor, apoyo y ejemplo. A mis hermanas y sobrinas por años de amor, aprendizaje y apoyo. Y al resto de mi adorable famlilia.

A CONACYT, que me ha apoyado financieramente para la realizacion de mis estudios.

A mi supervisor, Profesor Wuqiang Yang por su paciencia y su sabia direccion durante mis estudios.

A Michelle, por su compañia y a Luis por su amistad.

A México.

Chapter 1

Introduction

1.1 Background and motivation

1.1.1 Electrical tomography

Electrical capacitance tomography (ECT) and electrical resistance tomography (ERT) methods have been widely used to obtain information from different media in a broad range of applications such as industrial process monitoring (Wang et al., 1999) and multiphase flow measurement (Li t al., 2012), although both methods have proven their usefulness and a great number of researchers and institutions have their interest and time invested on ECT and ERT development, there is still existing a great opportunity to innovate and improve these well known methods by the design and use of new sensing techniques and hardware development.

Dual-modality tomography has appeared as a possible solution for the limitations on both electrical tomographic methods, exploiting the best characteristics of ECT and ERT. It is expected that the construction of a system with these advantages would fulfil the requirements for imaging complex media.

The ERT system proposed in this work is expected to improve the performance of currently used ERT systems which are not able to generate quantitative information of the conductive distribution and to be a first step towards the integration of a dual modality tomographic system. The system built is devised to exclusively image the conductive distribution of the media under study. This is done by adjusting the operating frequency to a level low enough to avoid the effect of the capacitive impedance in the current measurements. Therefore, at this stage of development, the proposed approach allows us to image only conductivity distributions at a low frequency. In addition, current ECT systems allow to image permittivity distributions at higher operating frequencies. Nevertheless, future development is expected to allow us imaging conductivity and permittivity distributions simultaneously at a single frequency with the use of a dual modality imaging system.

1.1.2 Motivation

Several researchers have reported the integration of ECT and ERT in a dual-modality system. Cui et al. (2009) developed a system integrating ECT and ERT with current-excitation and voltage-measurement sensors in the same sensor plane and using a sensing scheme of changing modality when one or another principles are required. Wang et al. (2014) reported the simulations tests, construction and operation of a sensor able to image both, conductivity and permittivity characteristics of the media simultaneously applying a voltage excitation. Marashdeh et al. (2007) reported the use of an ECT sensor to measure the permittivity and conductance characteristics of the media based in capacitance and power measurements.

A new approach for dual-modality tomography has been proposed by Sun and Yang (2015) with a voltage-excitation and current-measurement scheme, allowing to measure the conductive and dielectric materials' properties using an impedance analyser based system. This technique posses the capability to image a wide range of materials within the same electrode area and simultaneously.

On the other hand, it has been reported by Sun and Yang (2012) that in an ERT system with a current-excitation and voltage-measurement sensing scheme, small metallic pins are usually used as measuring electrodes and a severe 3D effect is seen. This leads to the electric field to spread out the electrode plane in an axial direction generating inaccurate measurements and image reconstruction errors.

The motivation to develop a dual-modality ECT/ERT system with a voltage-excitation scheme is that it would simplify the integration of ERT with ECT, allowing to get the conductive and capacitive measurements in parallel and with the use of the same internal electrodes. In consequence, the sensor's construction would be simpler and the frame rate could be increased due to the elimination of the need to change between both imaging modalities.

In addition to the latter mentioned motivations, it is foreseen that the development of ERT with voltage-excitation would reduce the fringe effect. Altogether, a simply circuit design would reduce cost and simplify a ERT implementation when a single modality imaging system is required.

1.2 Objectives of the project.

The objectives of this project are the following:

- To test the feasibility of imaging a non-conductive material over a conductive background using an experimental ERT voltage-excitation and current measurement.

- Design an improved ERT tomographic sensor with inner electrodes.

- Build an ERT system based on a Agilent data acquisition unit to image conductive media with voltage excitation.

- Perform a comparison between the two excitation and measurement approaches to implement ERT.

1.3   Thesis Outline

Chapter number 2 in this thesis is intended to present a summary regarding the basic principles of ECT and ERT. As well as an analysis of the advantages and disadvantages of this techniques in the application of multi-phase flow metering.

Chapter 3 presents the steps followed in the design of an ERT sensor and the set up for an ERT system with a voltage-excitation and current-measurement scheme.

Chapter 4 contains the description of the procedure to generate the conductivity sensitivity maps altogether with a report of the algorithms used to perform image reconstruction.

Chapter 5 summarises the results obtained during this research, and an analysis of such results is made.

Chapter 6 gives the conclusions drawn from this research and a suggestion of future work.

Chapter 2

Literature review

Electrical Tomography is a widely used imaging method due to its advantages like low cost, non-radiation and good temporal resolution. Two of the most popular electrical tomographic methods are ECT and ERT. In this chapter the most important and basic characteristics of both methods are discussed.

2.1 Electrical Resistance Tomography

ERT is a well known tomographic technique intended to get information of the electrical conductivity distribution within a space surrounded by metallic electrodes. These electrodes are placed evenly around the object to test. Two electrodes are used to drive an electrical current inside the region of interest and the remaining electrodes are used to measure the potential distribution on the object's boundaries. In this way, making use of a data acquisition hardware and a computer, an image can be reconstructed and it is possible to obtain a cross sectional view of the object being tested.

Figure 2.1 shows a typical set-up for a ERT system. The arrangement usually consists in a sensor composed by several metallic electrodes. The sensor is connected to a data acquisition system that includes the sensing electronics, a signal conditioning stage and a communication board to allow bidirectional data transfer between the computer and the DAQ. In this way, it is possible to reconstruct the conductivity distribution. In addition, this communication link allows to send control signals to the circuitry.

As a result of the need for electrical current flowing into te region of interest, the metallic electrodes are required to be in contact with the object to image. In consequence, ERT is an invasive but non-intrusive system. Figure 2.2 shows a typical construction of an ERT sensor with the metallic electrodes placed at equal radial distance in the same axial plane.

In the field of industrial process tomography, ERT is mainly used in the chemical
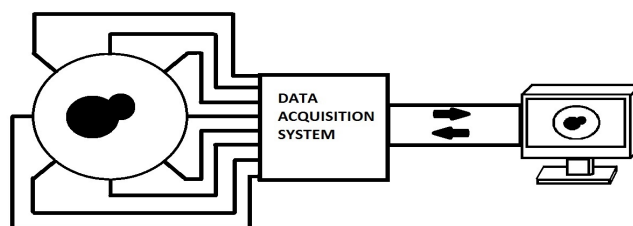
Figure 2.1: ERT system set-up

and petrochemical industry to monitor mixing operations (Yenjaichon et al., 2011) and multi-phase flow imaging (Loh et al., 1999) due to its ability of distinguishing materials with different conductivities, its low cost and high frame rate.
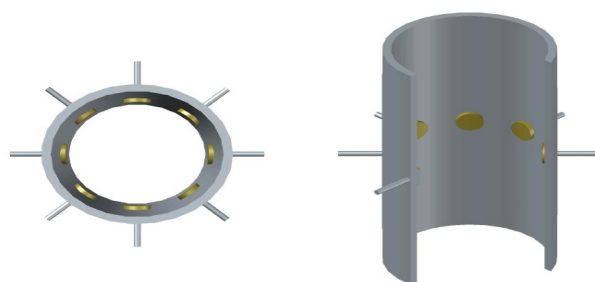
Figure 2.2: Typical ERT sensor construction

2.1.1   Sensing strategy

When imaging with an ERT system, a pair of electrodes are used to drive a sinusoidal AC current into the object to test, generating a potential distribution. Afterwards, the remaining electrodes are used to measure the voltage on the material's boundaries. The existence of a material with a different conductivity inside the area to be tested, generates a change in the potential distribution. Therefore, the voltage measurements can be used to obtain information about the material's distribution and therefore to perform image reconstruction.

In ERT there are three mainly used measuring strategies

- Adjacent electrodes strategy.

- Opposite electrodes strategy.

- Conducting Boundary strategy.

Adjacent strategy

In this measurement strategy, two adjacent electrodes are used to inject an AC current into the conductive material. Electrodes 1 and 2 are firstly set as excitation pair. Subsequently, the remaining electrodes are used in pairs to measure the voltage. The voltage is measured between electrodes 3 - 4, 4 - 5,... until all the remaining electrodes pairs are used. Afterwards, the next adjacent electrodes, in this case 2-3, are set as excitation electrodes and the voltage is measured in between the remaining electrodes, 4-5, 5-6,... until all the independent measurements are taken.

This strategy yields M number of independent measurements, the relation between M and the number of electrodes N is given by:

$$M = \frac{N(N-3)}{2} \tag{2.1}$$

As an example, if an ERT sensor as the shown in Figure 2.3 with a N number of 8 electrodes is used, the maximum number of independent measurements M accordingly to equation 2.1 would be M=20.

As a result of the use of this strategy, the current flows in between adjacent electrodes near to the object's boundary. Therefore, the sensibility in the central part of the object is reduced in comparison with the sensibility shown in the boundaries.
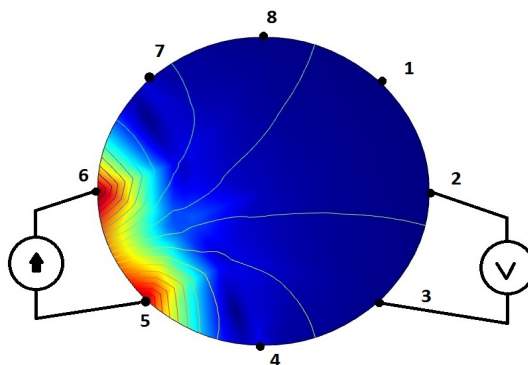
Figure 2.3: Adjacent strategy showing the potential distribution.

Opposite strategy

To perform the measurements with an ERT system using this strategy, two diametrically opposite electrodes are selected as the excitation electrodes. In this case, electrode 1 and 5 for an 8 electrodes system. Eventually, an electrode adjacent to the electrode used to inject current is selected as voltage reference, in this case electrode 2 and the voltage measurement is performed with the remaining electrodes. Afterwards, the next opposite excitation electrodes are selected in a clockwise rotation, e.g., electrodes 2 and 6, and the voltage measurements are taken with the reference electrode number 3. This rotation is repeated until all the independent measurements are collected.

When using an 8 electrodes sensor like the one depicted in figure 2.4 with an opposite sensing strategy it is possible to obtain five voltage measurements for each current injection. Therefore it is possible to obtain 8x5=40 measurements, from which only 18 are independent.
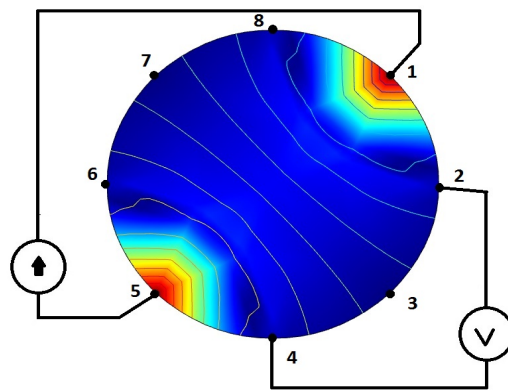
Figure 2.4: Opposite strategy showing the potential distribution.

This strategy yields less independent measurements in comparison to the adjacent strategy. This means the image reconstruction is performed with less information and the image quality is decreased. Nonetheless, the use of opposite electrodes generates a more uniform current distribution (Harikumar et al., 2013). Therefore, the sensibility is more evenly distributed within the sensing area. In contrast, as the current flows mainly through the central area, the sensibility on the areas near to the boundaries is reduced compared to adjacent strategy.

Conducting Boundary strategy.

Usually, ERT sensors are built in a way that the metallic electrodes are mounted over a non-conductive material, for example a plastic vessel or pipe. When it is required to mount an ERT sensor in metallic vessels or pipes, this strategy can be used to perform the required measurements. With this configuration only one pair of electrodes are used at once, one electrode to drive in the AC current, the another one to measure

the voltage in the vessel's boundary. For both, the voltage measurement and current injection, the metallic grounded walls are taken as reference. This process is repeated until all the possible independent measurements are taken. Figure 2.5 shows an 8 electrodes ERT system in a vessel/pipe with conductive walls.
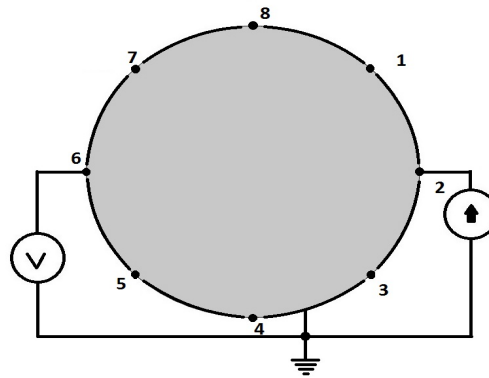
Figure 2.5: Conductive boundary strategy.

As shown by Wang et al. (1994) when using the conducting boundary strategy, the maximum number of independent measurements *M* with a *N* number of electrodes is given by:

$$M = \frac{N(N-1)}{2} \tag{2.2}$$

For example, if an ERT sensor as the shown in Figure 2.5 with a *N* number of 8 electrodes is used, the maximum number of independent measurements *M* accordingly to equation 2.2 would be *M*=28.

In particular, when using an ERT sensor with the same number of electrodes, the conductive boundary strategy yields the higher number of independent measurements.

As a result of the existence of a substantial grounded area when using this strategy, the sensitivity in the area near to the electrodes is high and it decreases rapidly towards the centre of the sensing area (Wang et al., 1994).

2.1.2 Hardware set-up

Sensor design

Although sensor design considerations are usually focused to every specific application, there are general characteristics that need to be consider on every sensor design.

- Electrode material.

  It is important to consider that the chosen material to build the electrodes should withstand a different range of temperatures, pressure, material's PH and corrosive materials. Also, the material has to be more conductive than the materials to be imaged in order to obtain a useful measurement (Dikin and Wang, 1996).

- Electrode shape.

  There are three types of electrode shapes with different characteristics, pros and cons in ERT (Hao et al., 2013). The rectangular shape, the small pin electrode and a mixture of both of them.

  The rectangular electrode, as its name states is made by a thin rectangularly shaped metallic sheet fixed in the inner side of the pipe or vessel wall. The radial size of this electrodes is principally determined by the number of electrodes in the sensor arrangement. The axial size of these electrodes is determined by the designer, and it could go from few centimetres to a dozen or more centimetres. This type of electrode possess the advantage of generating a more uniform current flow inside the media to be imaged. In the other hand, a drawback of using this rectangular shaped electrodes is that the voltage measurement is not only function of the potential distribution in the sensing plane.

  The pin electrode type consists of a small metallic round plate. The electrodes of this type are also mounted in the inner face of the pipe or vessel wall to be in contact with the material at the interior of the sensor structure. The diameter of electrodes is usually less than 1 cm, in an attempt to get a voltage measurement from a small area, allowing in this way to get a voltage measurement from a single point in the sensing plane. However, when these electrodes are used to drive the current in the material to be imaged, the sensing field spreads out in a non uniform way, generating a severe fringe effect (Sun and Yang, 2012).

  The compound electrode features the best characteristics of the rectangular and pin electrodes. It is built with a big rectangular electrode used to drive the current into te media to be imaged, generating a more uniform sensing field, and a small pin electrode to measure a punctual voltage value. The principal drawbacks of this approach are the complexity and cost of building such a complex sensor.

- Driven guards

  The construction of an ERT sensor with the inclusion of driven guards consists in the placement of a series of metallic plates in both axial ends of the sensing electrodes. These driven guards are driven with the same current as the sensing

electrodes. Therefore, the driven guards have to be placed in the inner face of the pipe wall in contact with the conductive material.

The driven guards in ERT are aimed to build a more uniform electric field inside the sensor area and to constrict the sensing area within the sensing electrodes plane (Ma et al., 1999).

A disadvantage for the use of internal driven guards is that they have to be in the inner face of the pipe wall, making the sensor construction more complicated.

- Mounting pipe or vessel.

  In order to hold the electrodes in a fixed position it is necessary to use a mounting material, usually a pipe or a vessel's wall. An important consideration regarding the sensor design is the selection of mounting material. The mounting case for the electrodes has to be adequate to every process and withstand a variety of temperatures and pressures. A plastic container is used due to its low cost and ease to work with it. In contrast, a great number of industrial applications require the use of metallic containers or pipes.

Voltage controlled current source (VCCS)

Imaging conductive materials with an ERT system requires the use of current source with a high output impedance and capable to deliver a high quality sine wave AC current to a variety of different loads. A widely used voltage-controlled current source (VCSS) in ERT is the Howland current source (Bian et al., 2012).
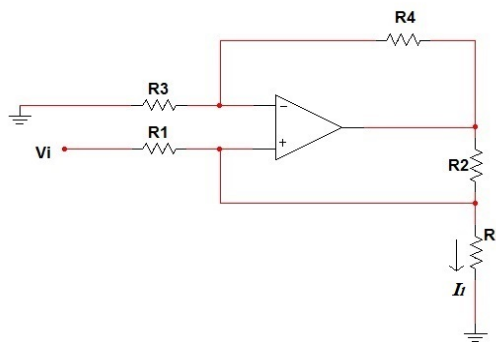
Figure 2.6: Howland current source.

$$\begin{cases} Il = \dfrac{Vi}{R_1} \\[2mm] \dfrac{R_1}{R_2} = \dfrac{R_3}{R_4} \end{cases} \tag{2.3}$$

Equation 2.3 gives the relationship between the voltage supplied to the inverting terminal and the current delivered to the load. As can be seen, the value of the current delivered to the load, depends only on the input voltage and the input resistor R_1. In other words, the amount of current flowing through R_L not depends of the value of R_L.

An improvement of the Howland current source named as Advanced Current Source has been developed (Zhangyong et al., 2010). The improvement consist of the addition of a feedback resistor R_5 as seen in Figure 2.7. This feedback resistor allows to increase the output impedance.
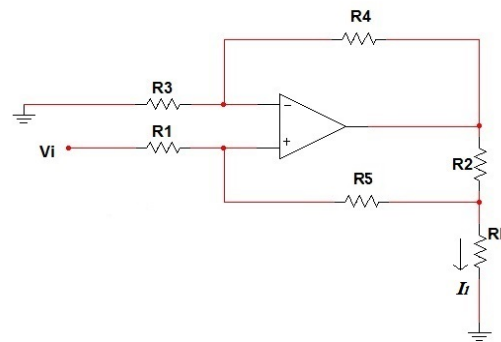
Figure 2.7: Advanced Howland current source.

$$
\begin{cases}
Il = \dfrac{Vi}{R_2} \\[2mm]
R_3 = (R_1 + R_2) \\[2mm]
R_1 = R_4 = R_5
\end{cases}
\qquad (2.4)
$$

Equation 2.4 states the relationship between the voltage supplied to the inverting terminal and the current delivered to the load. As it can be seen, the value of the current delivered to the load, depends only on the input voltage and the resistor R_2. In other words, the amount of current flowing through R_L not depends of the value of R_L.

Voltage measurement

Voltage measurement in ERT is usually performed with a instrumentation amplifier, measuring the differential voltage between the two sensing electrodes when using the

adjacent method (Bhattacharyya et al., 2013), or referring the non-inverting terminal to ground when a single electrode detection is use, for example when imaging using the conductive wall strategy.

2.1.3   Forward problem in ERT

Forward problem

The forward problem on ERT consists in the determination of the boundary voltages due to a given electrical conductivity distribution and current density on the driven electrodes. To solve this problem, it is required to know the mathematical model describing the electric field inside the area to be imaged.

The frequency of the sine wave AC current injected into the sensing area is usually low enough to neglect the effects of magnetic fields and the dielectric properties of the materials. Therefore, the phenomenon inside the sensing area can be described by the Poisson's equation with Neumann boundary conditions (Ma et al., 1997):

$$\begin{cases} \nabla \cdot [\sigma \nabla \phi] = 0 \\[2mm] \sigma \cdot \frac{\partial \phi}{\partial n} = J & \text{on source electrode} \\[2mm] \sigma \cdot \frac{\partial \phi}{\partial n} = -J & \text{on sink electrode} \\[2mm] \sigma \cdot \frac{\partial \phi}{\partial n} = 0 & \text{on other electrodes} \end{cases} \tag{2.5}$$

In equation 2.5 J is the current driven into the area to image, σ is the electrical conductivity, ϕ is the electric potential. In order to solve Poisson's equation and obtain the potential distribution due to the current density and the electrical conductivity distribution a FEM solver is usually used. A CAD model of the sensor's geometry is build and the boundary conditions are set.

Figure 2.8(a) shows the potential distribution calculated using COMSOL FEM solver. Figure 2.8(b) depicts the mesh used to solve the system. Figure 2.8(c) illustrates the potential distribution due to a phantom. In the 2D phantom depicted in Figure 2.8(d) the grey area is set as a conductive material with an electrical conductivity of 5.5e-6[S/m] and the central blue circle is set as a non-conductive material.

The FEM solver allows to get the potential distribution due to a different type of electrical conductivity distributions. This facilitates image reconstruction from simulated data and the test of different electrode arrangements.

(a) Potential distribution   (b) Mesh

(c) Potential distribution   (d) 2D Phantom
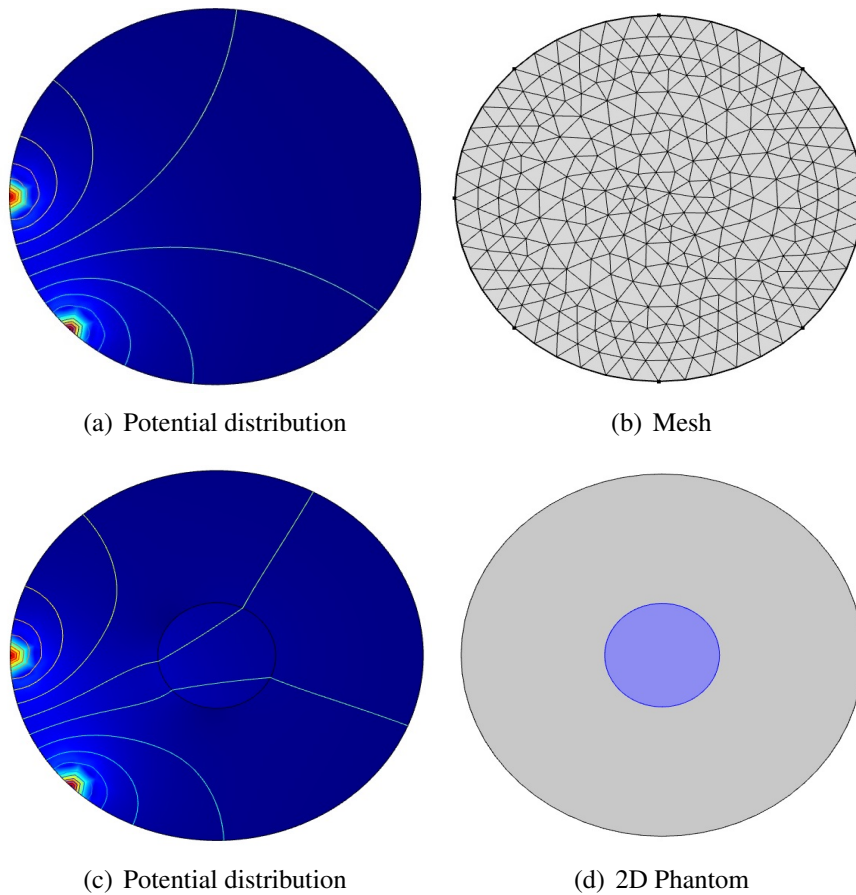
Figure 2.8: ERT potential distribution and phantom from FEM solver.

The linearised and discrete form of the forward problem can be described by

$$B_{(Mx1)} = S_{(MxP)} \cdot G_{(Px1)} \tag{2.6}$$

where B is a vector containing the expected voltage measurements in the system's boundaries. S is the sensitivity map and G is the vector containing the conductivity values for each pixel in the image.

Sensitivity maps

The sensitivity matrices are a representation of the sensor's response to an individual stimulus in the sensing area. Although the sensitivity maps in ERT can be measured directly form the sensor using a material with different conductivity than the background and gathering the response form every electrode pair, a more practical and fast way to obtain the sensitivity maps is to calculate them form (Zhang, 2011)

$$S_{i,j}(x,y) = -\int_{p(x,y)} \frac{\nabla \phi_i}{A_i} \frac{\nabla \phi_j}{B_j} dxdy \tag{2.7}$$

where ϕ_i is the potential due to i electrodes driving the current. ϕ_j is the potential generated due j electrodes driving the current. A_i and B_J are the currents driven by each electrode pair.

2.1.4   Inverse problem in ERT

Inverse problem

In ERT the inverse problem consists in the determination of the electrical conductivity distribution from the voltage measurements on the system's boundary.

Image reconstruction algorithms

After the voltage measurements have been taken, it is possible to perform image reconstruction to obtain an image representing the conductivity in the cross section of the sensor.

Some of the most popular reconstruction algorithms used in ERT are the following:

- Linear Back Projection LBP

   Linear back projection (LBP) is an one step image reconstruction algorithm focused in the determination of the conductivity vector from equation 2.6. As the number of independent measurements is considerably less than the number of pixels, the matrix S is a not square. Therefore, the conductivity vector cannot be calculated by

$$G = S^{-1}B \tag{2.8}$$

   In consequence, an approximation of the conductivity vector $\hat{G}$ should be calculated by the use of the transpose of the sensitivity maps S^T from

$$\hat{G} = S^T B \tag{2.9}$$

The approximate normalized conductivity $\hat{G}(k)$ for each pixel can be calculated from (Dickin and Wang, 1996)

$$\hat{G}(k) = \frac{\sum\limits_{i=1}^{m} B_i S_i(k)}{\sum\limits_{i=1}^{m} S_i(k)} \quad \text{for } k = 1, ..., p \qquad (2.10)$$

where B_i is the normalized voltage change measured at the electrode pair i. S is the sensitivity map for each electrode pair. And m is the number of independent voltage measurements.

The Linear back projection algorithm has the advantages of being a fast, single step image reconstruction method. Additionally, its implementation does not require large computational resources. Therefore, it is usually used when real time image reconstruction is required. Figure 2.9 shows the procedure followed to implement a Linear Back Projection LBP algorithm.
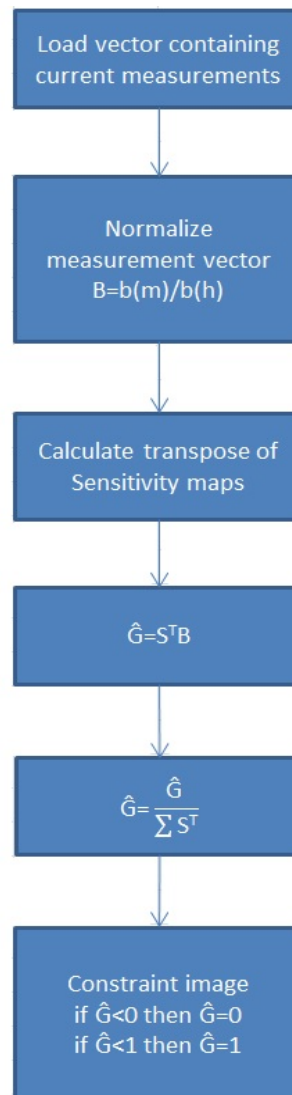
Figure 2.9: Linear back projection flow chart

- Landweber

Landweber is an iterative image reconstruction algorithm that consists in the actualization of the conductivity vector on each iteration. The first conductivity vector is obtained by the application of LBP. Afterwards, the forward problem is solved on each iteration to obtain the voltage due to the actual conductivity vector. Finally, the conductivity vector is updated by the image obtained from the linear back projection of the difference between the vector containing the measured voltages and the voltage vector from the solution of the forward problem (Yang et al., 1999).

$$\begin{cases} \hat{G}_0 = S^T B \\ \hat{G}_{k+1} = \hat{G}_k + \alpha S^T (B - S\hat{G}_k) \end{cases} \tag{2.11}$$

where $\hat{G}$ is the approximation of the conductivity vector. S is the sensitivity map. B is the vector containing the normalized voltage measurements. α is a constant called relaxation factor that helps to control the convergence rate.

A drawback of the Landweber iterative algorithm is its poor convergence property. A modification has been introduced into the algorithm to improve the convergence property, resulting in the projected Landwaber algorithm (Yang and Peng, 2003).

$$\hat{G}_{k+1} = P[\hat{G}_k + \alpha S^T (\lambda - S\hat{G}_k)] \tag{2.12}$$

where

$$P[f(x)] = \begin{cases} 0 & \text{if} \quad f(x) < 0 \\ f(x) & \text{if} \quad 0 \leq f(x) \leq 1 \\ 1 & \text{if} \quad f(x) > 1 \end{cases} \tag{2.13}$$

P works as a constraint, assuring that the permittivity values in the reconstructed image are in between the upper and lower boundaries.

The Landweber iteration gives a more accurate estimation of the conductivity distribution from the measured voltage differences. A disadvantage of this algorithm is that is time consuming. Figure 2.10 depicts the Landweber algorithm.
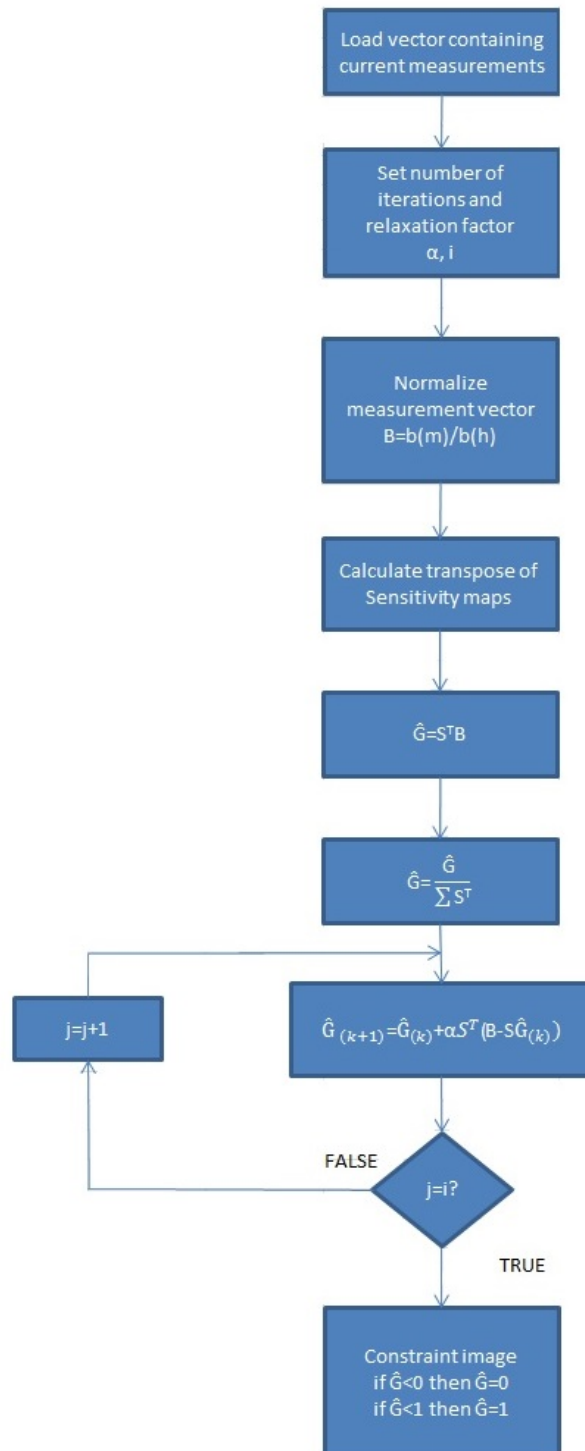
Figure 2.10: Landweber flow chart

2.2   Electrical Capacitance Tomography

ECT is a tomographic technique focused to detect permittivity changes inside the sensing area. The detection is made by the measurement of the capacitance values between the electrodes surrounding the area to be imaged. The measurements are gathered by a data acquisition system and image reconstruction can be performed with a computer.
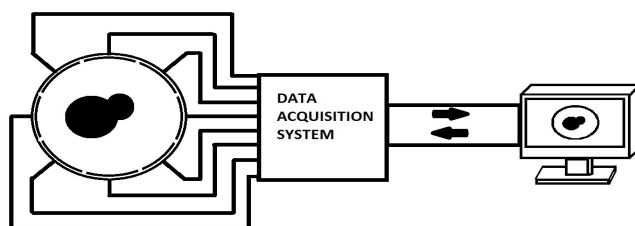
Figure 2.11: ECT system set-up

Figure 2.11 depicts the structure of a typical set-up for an ECT system. The arrangement usually consists in a sensor composed by several metallic electrodes. The sensor is connected to a data acquisition system that includes the sensing electronics, a signal conditioning stage and a communication board to allow bidirectional data transfer between the computer and the DAQ stage. In this way, it is possible to reconstruct the permittivity distribution. In addition, this communication link allows to send control signals to the circuitry.
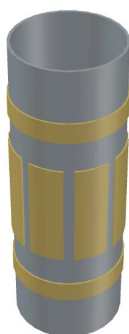
Figure 2.12: Typical ECT sensor with external electrodes and earthed ring

Figure 2.12 shows the typical ECT sensor. These sensors are usually built with metallic electrodes evenly mounted around the outer face of a pipe or vessel wall.

2.2.1 Sensing strategy

With an ECT system, capacitance measurements are taken between two electrodes at every time. The driving electrode is set to an AC voltage, say electrode number 1, and the detecting electrode is set to a virtual ground, in this example electrode number 2, by means of the inverting input of an operational amplifier. The remaining electrodes are set to ground to avoid charge injection between the detecting electrode and the rest of unused electrodes. Afterwards, the electrode set in the sensing mode, electrode 2, is connected to ground and the next sensing electrode, electrode number 3, is connected to virtual ground. This process is repeated until all the possible measurements are taken between the driven and the sensing electrodes. Next, the electrode adjacent to the first electrode set in driving mode is connected to the AC voltage and the measurements are taken. This sequence is followed until all the independent measurements are gathered (Yang et al., 1995).

Figure 2.13 shows the way ECT measurements are performed between electrodes 1-2 and 1-3.

(a) 1-2 electrodes measurement   (b) 1-3 electrodes measurement
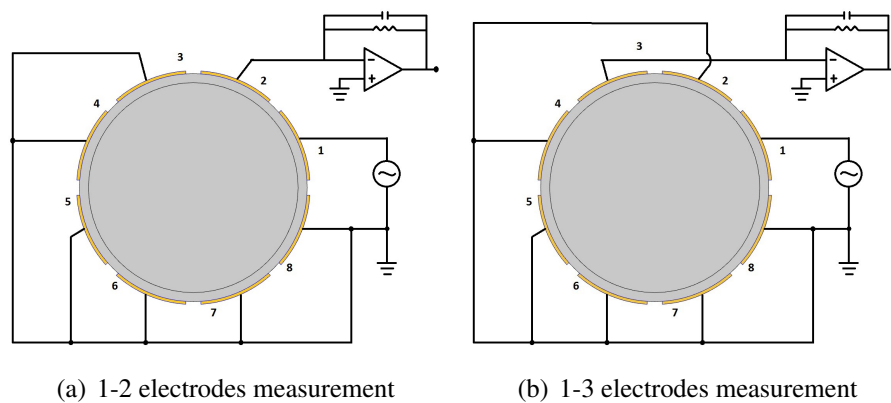
Figure 2.13: ECT sensing protocol.

The number of independent measurements *M* in ECT is given by:

$$M = \frac{N(N-1)}{2} \tag{2.14}$$

Where *N* is the number of electrodes. In this way, with an ECT sensor built with 8 electrodes, the maximum amount of independent measurements is 28.

Table 2.1 shows the measurement sequence for an ECT system with 8 electrodes. There are two numbers in every cell, the number in the left represents the number of the sensor being the driving electrode. The number in the right represents the number

of the sensing electrode. i.e. for all the measurements in the far left column the driving one is the electrode number 1, and the sensing electrodes are 2, 3, 4, 5, 6, 7, 8. This process is repeated changing the driving electrode until the 28th measurement is taken. This measurement is represented in the far right cell with the electrode pair 7 - 8.

1-2	2-3	3-4	4-5	5-6	6-7	7-8
1-3	2-4	3-5	4-6	5-7	6-8	
1-4	2-5	3-6	4-7	5-8		
1-5	2-6	3-7	4-8			
1-6	2-7	3-8				
1-7	2-8					
1-8						

Table 2.1: Measurement sequence for an 8 electrodes ERT sensor

2.2.2   Hardware set-up

Sensor design

ECT allows two types of configurations for the sensing technique (Yang, 2010).

- External electrodes

  An ECT sensor with external electrodes is built by the fixation of metallic plates in the outer side of the pipe or vessel. In consequence of this type of electrode mounting, ECT with external electrodes become a non-invasive and non-intrusive imaging technique.

  In this way, some advantages of this sensor type are the ease of construction and the characteristic of being a non-intrusive imaging technique. Also, the electrodes being outside the container, do not have to withstand the severe conditions like high temperature, pressure or abrasives that could be involved in the process being monitored. A drawback of an ECT sensor with external electrodes is the capacitance of the pipe wall affecting the measurements and the large standing capacitances (Yang, 1997).

- Internal electrodes

  An ECT sensor with internal electrodes is assembled by the mounting of the metallic plates in the inner face of the pipe or vessel wall. Therefore, ECT with

internal electrodes is an invasive, non-intrusive imaging technique. The main advantage for the use of an ECT sensor with internal electrodes is the high sensibility due to direct contact with the material to be imaged. Some disadvantages of this sensor construction are that the sensing becomes invasive. Also, the difficulty of construction and the fact that the electrodes are in contact with the process, being exposed to harsh environment and materials.

• Number of electrodes.

The determination of the number of electrodes in ECT is a trade-off between spacial resolution, capacitance values, data acquisition speed and circuitry complexity (Yang, 1997). The more electrodes are used, the smaller is the electrode's size. For a given pipe's diameter, there is a fixed circumference. Therefore, the increase of the number of electrodes would represent the downsize in the radial dimension for all the electrodes in order to be fitted around in the same circumference. In consequence, the inter-electrode capacitances would be reduced, making in this way more difficult the measurement of such capacitances. Furthermore, the increase on the number of electrodes would represent in a proportional increase of measurement channels. As result, a more complex and expensive data acquisition system would be needed. In addition, the imaging speed would be reduced due to the increased number of independent measurements and data to be processed.

On the other hand, the increase on the number of electrodes would allow to gather more independent measurements, yielding in this way more information for the image to be reconstructed. Due to the latter mentioned considerations, the number of electrodes used in most ECT systems are 8 or 12 (Yang, 1997).

• Axial length of electrodes.

This is an important parameter to consider due to its implications in image quality. The larger the electrodes, the larger is the inter-electrode capacitance and the sensing circuitry does not need to be extremely sensitive. In addition, the fringe effect is reduced due to the more even distribution of the electric field in the sensing area. In contrast, too long electrodes would limit the size of the smallest piece able to detect by the system. Furthermore, the construction of an ECT sensor with very large electrodes would be impractical due to the limited space in real applications. In opposite, the length of the electrodes cannot be reduced without considering two key aspects, the first one is the sensitivity of the circuitry measuring the capacitance. This is, if the electrodes are too short in the axial direction, the inter-electrode capacitance would be considerably reduced and a highly sensitive circuitry would be required. In practice, there is a limit on the smallest capacitance that can be measured for an ECT application. The second reason is the fringe effect seen in the axial ends of the electrodes. When reducing the electrode's axial length, the electric field spreads out the sensing

area generating errors in the reconstructed image. Therefore, it is usual to select electrodes with an axial length greater than the sensor's diameter, commonly two-fold, in this way it is possible to neglect the fringe effect (Yang, 2010).

- Driven guards

  Some researchers have proposed the use of an ECT sensor with driven guards. The construction of such sensor consists in the placement of either internal or external electrodes in the pipe wall. Additionally, two sets of driven guards are mounted symmetrically on both axial ends of the sensing electrodes. These guards are connected to the same potential as the sensing or driving electrodes. The driven guards are aimed to allow the use of shorter sensing electrodes (Yang, 2010). A drawback for the use of driven guards is their influence into the capacitance measurement. In other words, the capacitance measurement would not be only function of the inter electrode capacitances. Rather, it would be also influenced by the inter capacitance between the sensing electrode and the driven guards in both axial directions. In addition, it has been show that the increased length of the driven guards extends the sensing area in the axial direction (Yan et al., 1999).

- Earthed screens

  There exist tree types of earthed screens used in ECT sensor construction.

  The first, consists in a metallic screen coveting the whole external pipe's circumference and extending beyond the electrodes in axial directions. The main function for this earthed screen is to shield the sensor form external noise and interferences.

  The second type, is built with metallics rings that are fixed some millimetres away the electrodes in both axial directions. The rings' purposes are to reduce noise in the capacitance measurements and the constraint of the sensing field in the axial direction as an attempt to reduce the fringe effect (Sun and Yang, 2014).

  The third type of earthed guards are the radial guards. This guards are meant to reduce the value of the inter electrode capacitance in adjacent electrode pairs. A drawback for the use of this kind of guards is the difficulty of construction.

- Sensor shape

  In industry and laboratories a great number of tanks, vessels and pipes are circular. That is why the usual shape adopted for an ECT sensor construction is circular. In contrast, some specific applications require the construction of a

non-circular sensor. It has been reported the construction of ECT sensors with a square shape for the application on fluidised beds (Yang and Lui, 1999).

Capacitance measurement and switching circuit

Every electrode on an ECT system has a dual functionality, as driving and detecting electrode. While performing as driving electrode, an AC voltage is applied to such electrode. Whereas it is acting as detecting electrode, it is connected to a measuring circuit, allowing to measure the electrical properties of the materials inside the sensor area. The electrode's dual functionality requires a switching arrangement to allow the electrode to perform its functions correctly.

Figure 2.14 shows the switching stage and measuring circuit. One of these arrangements is used for each electrode. When the switches J2, J1 and J6 are closed and the remaining switches are open, the electrode is set to excitation mode. When the switches J5, J4 and J3 are closed and the remaining switches are open, the electrode is set to detecting mode (Styra and Babout, 2010). This switching arrangement has the advantage of reducing charge injection due to the switch's capacitance.
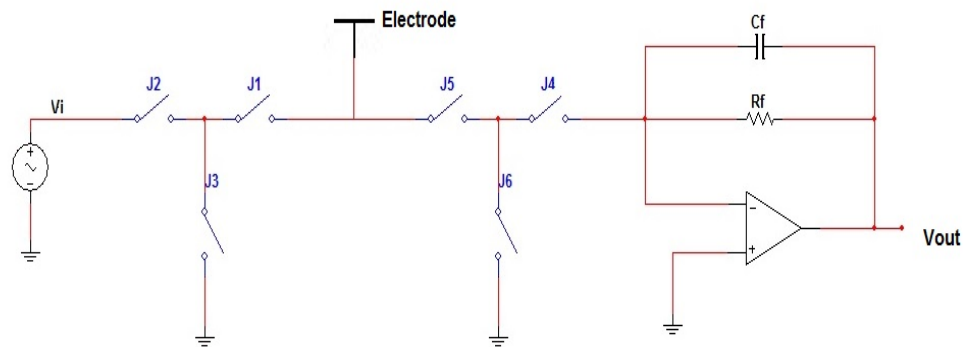
Figure 2.14: Switching stage and measuring circuit

When the electrode is in detecting mode, the AC current flowing towards and from the electrode is measured to determine the capacitance between such electrode and the driving electrode. The way of doing this is with the use of a charge amplifier. Among the various advantages of this measuring circuit are, its low-cost and ease to build. Nevertheless, its most important feature is being a stray-free capacitance meter (Kuroda, 1983).

As can be seen in Figure 2.15, the stay capacitance Cs1 is driven directly by the power source. In consequence, it does not affect the measurement of the desired capacitance

Cx. Additionally, the stray capacitance Cs2 is referred to both input terminals of the operational amplifier, and due to the negative feedback implemented in the circuit, there is no potential difference driving the capacitance Cs2. As a result, there is no affectation in the measurement due to the capacitance Cs2.
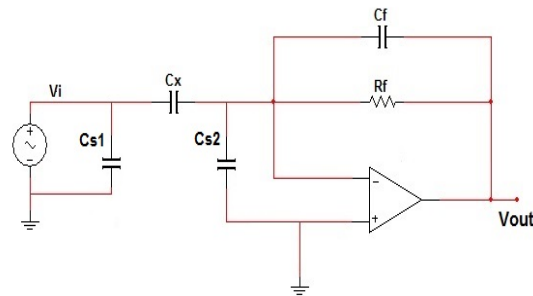
Figure 2.15: Measuring circuit

The capacitance Cx can be determined directly from the voltage output and the feedback impedance by the following relationship:

$$Cx = \frac{(Cf * Rf + Cf)Vout}{Rf * Vi} \tag{2.15}$$

The relationship described by 2.15 remains valid for a Vi with a frequency set in the central area between $\dfrac{1}{2\pi Cf * Rf}$ and the upper limit of the operational amplifier's bandwidth (Kuroda, 1983).

2.2.3   Forward problem in ECT

Forward Problem

The forward problem in ECT consists of the determination of the inter-electrode capacitances form a given permittivity distribution. An FEM solver is usually used to perform this calculation.

The frequency of the AC voltage used to excite the sensor is low enough to generate a wave length considerably larger than the sensor's size. Thus, it is possible the use

of quasi-static approximation of Maxwell's equations (Marashdeh et al., 2007). In addition, an assumption is made when solving the forward problem with a 2D model. The fringe effect due to a finite axial length of the electrodes is not considered, meaning that it is assumed that the electric field is homogeneous in the axial direction (Khan, 1993). Therefore, the mathematical model reigning the area within the sensor can be described by Poisson's equation 2.5 as described in section 2.1.3

A 2D CAD model of the sensor filled with a homogeneous permittivity distribution is built, a mesh is generated and the problem is solved, yielding as a result the potential distribution inside the sensor due to the given permittivity distribution.

(a) Potential distribution

(b) Mesh

(c) Potential distribution
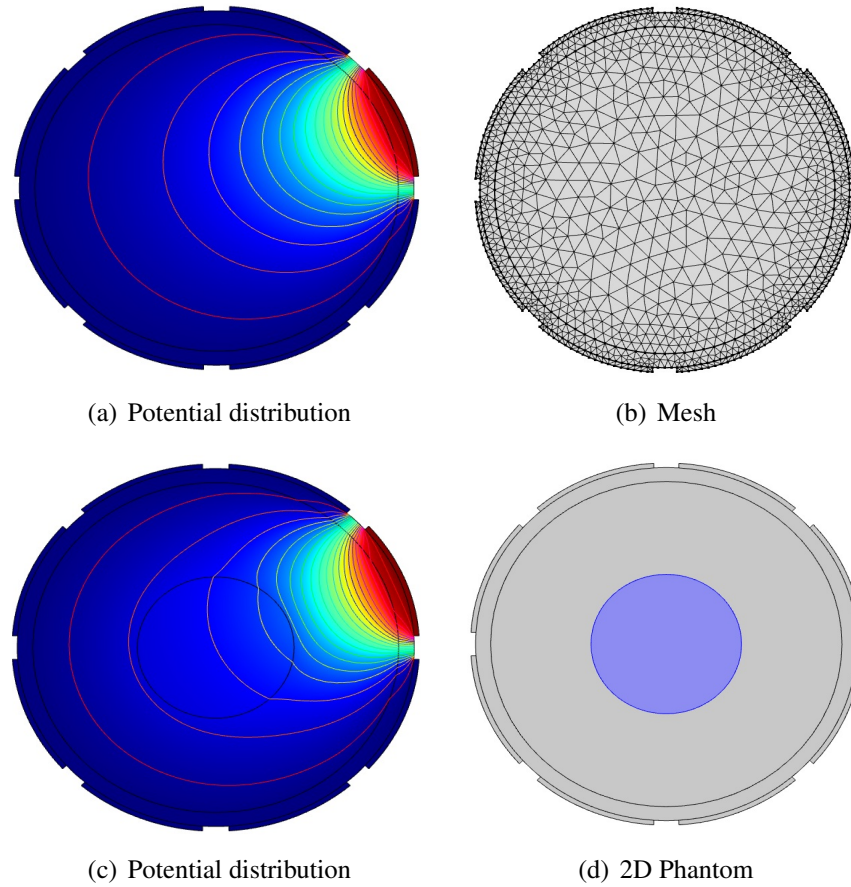
(d) 2D Phantom

Figure 2.16: ECT potential distribution and phantom from FEM solver.

Once the potential distribution inside the sensor area is calculated using the FEM solver, the charge Q in any given electrode can be calculated by means of the Gauss' Law (Kim et al., 2007).

$$Q = - \oint_{\Gamma} \varepsilon(x,y) \nabla \phi(x,y) d\Gamma \tag{2.16}$$

In equation 2.16 Γ is the electrode surface, $\phi(x,y)$ is the potential distribution and $\varepsilon(x,y)$ is the permittivity distribution. Once the charge Q on the detecting electrode is known, the inter-electrode capacitance can be calculated by:

$$C = \frac{Q}{V} = -\frac{1}{V} \oint_{\Gamma} \varepsilon(x,y) \nabla \phi(x,y) d\Gamma \tag{2.17}$$

Where C is the inter-electrode capacitance, and V is the voltage between the two electrodes. As usually the sensing electrodes are refereed directly to ground or virtual ground, V is the voltage applied to the driving electrode.

Due to the large amount of time and computational resources required to solve the forward problem by means of a FEM solver, it is not practical to implement image reconstruction algorithms with this technique, especially when the imaging speed is a key factor of the system's performance. An alternative for solving the forward problem in a faster way is the use of a method called Linear Forward Projection (LFP). This technique consist in the linearisation of the problem by use of the superposition theorem (Marashdeh et al., 2006). This is, the sensor response to a big stimulus can be determined from the addition of the individual response to a large amount of small stimuli. A sensitivity matrix for every electrode pair is created.

Based on the Linear Forward Projection technique, the linearised and discrete form of the forward problem can be described by the equation 2.6. Where B is a vector containing the M independent inter-electrode capacitance measurements, S is the sensitivity map, G is the image representing the permittivity distribution and P is the number of pixels in the image (Marashdeh and Teixeira, 2004).

Sensitivity maps

In an ECT system there are the same number of sensitivity maps as independent capacitance measurements. Thus, the number of sensitivity maps is directly determined for the number of electrodes in the ECT sensor. Each matrix represents the electrode pair response to a stimulus inside the sensor area. In other words, every sensitivity map stores a value for each pixel defined in the sensing area. This value is proportional to the inter electrode capacitance change due to a such pixel filled with high permittivity material whereas the rest of the pixels are filled with low permittivity material.

The sensitivity distribution $S_{i,j}(k)$ for the electrode pair i, j can be described as (Xie et al., 1992)

$$S_{i,j}(k) = \frac{C_{i,j}^m(k) - C_{i,j}^l}{C_{i,j}^h - C_{i,j}^l} \frac{1}{\varepsilon h - \varepsilon l} \tag{2.18}$$

Where $C_{i,j}^m(k)$ is the inter electrode capacitance when the *kth* pixel has a higher permittivity than the rest of the pixels. $C_{i,j}^l$ is the inter electrode capacitance measurement when the sensor area is completely filled with low permittivity material. $C_{i,j}^h$ is the inter electrode capacitance measurement when the sensor is full with high permittivity material. εh and εl are the permittivity values for the high and low permittivity materials respectively.

The sensitivity maps can be determined directly from the physical sensor. This is done by placing a probe, usually a plastic rod, in different adjacent positions throughout the sensing area and recording the sensor's response to such probe. The smaller the rod's diameter, the more information can be gathered but the capacitance change becomes too small to be measured. In an opposite way, if the diameter is too big, the less measurements are required but the resolution of the reconstructed image would be poorer (Yang and Conway, 1998).

This technique for the generation sensitivity maps has several disadvantages, first, to obtain useful sensitivity maps, the rod's diameter should be small. In consequence, the capacitance change due to the perturbation is vary small, so it is necessary to have a very sensitive data acquisition hardware. In addition, the placement of the material should be very precise, and the position changes are very small in both coordinates. Thus, a complicated apparatus is required to place the material in each position precisely. Furthermore, a large time is required to perform the sensitivity matrices.

Due to the obvious disadvantages of measuring the sensitivity maps directly form the sensor, a different approach has been proposed. An FEM solver can be used to obtain the potential distribution generated by one electrode on driving modality and the rest of electrodes as detection electrodes. From the potential distribution, the electric field can be calculated and the sensitivity maps can be obtained from equation 2.7 where $\vec{E}_i(x,y)$ is the electric field generated when the i electrode is in driving modality excited with a Ai voltage. $\vec{E}_j(x,y)$ is the electric field generated when the j electrode is in driving modality excited with a voltage Bj. Whereas p(x,y) is the area of a pixel in the position (x,y) inside the sensing area.

2.2.4   Inverse problem in ECT

Inverse problem

The inverse problem in ECT consists in the determination of the permittivity distribution from the measurements taken on the sensor's boundaries.

Image reconstruction algorithms

Once all the capacitance measurements are gathered and the sensitivity maps are calculated, it is possible to reconstruct an image showing with a color scale the permittivity distribution inside the sensor.

Two of the most accepted image reconstruction algorithms in ECT imaging are the linear back projection and Landweber algorithms.

The linear back projection is broadly used due to its speed. Being a single step algorithm it is possible to perform on line image reconstruction to obtain a qualitative description of the media under study. The LBP algorithm is implemented for ECT with equation 2.10 as described in section 2.1.4

The Landweber algorithm is used to obtain quantitative information regarding the media under study. Being an iterative algorithm is time and resources consuming. Therefore is not usually used for on-line image reconstruction. The projected Landweber algorithm is implemented for ECT with the use of equations 2.12 and 2.13 as described in section 2.1.4

2.3   Dual-modality electrical tomography

Dual modality tomography is focused to take advantage of the best characteristics of two tomographic techniques. This mixture of imaging techniques is intended to be able to image a wide range of different materials with a variety of characteristics.

This section is dedicated to the analysis of dual modality tomographic systems making use of ECT and ERT techniques.

It has been reported the construction and test of two main different dual modality tomographic systems. The first type is conformed for systems integrating ECT and ERT electrodes in the same sensor, either in different or the same sensor plane. The second type of systems are characterized by performing both conductance and capacitance measurements with the same electrodes, either simultaneously or subsequently one after other.

In the category of tomographic systems integrating ERT and ECT electrodes in the

same sensor are the following works and techniques.

The development of a multi modality tomographic system was announced by Qiu et al. (2007). The ERT and ECT electrodes in this system are located in different axial planes, avoiding in this way interferences between the two modalities. Altogether, the placement of the sensors in different axial planes makes the sensor construction less complicated. In addition, there is a dedicated data acquisition hardware for every tomographic modality. After the measurement are gathered, the images are reconstructed separately and processed. Afterwards, the data form the two different sensors is fused to get the complete information available from ERT and ECT modalities.

An advantage of this system set-up is the avoidance of interference between modalities and the possibility of taking measurements with both modalities simultaneously. Some drawbacks of this technique are that the measurements are not taken in the same axial plane, generating in this way incongruence in the data fusion. Additionally, there is required dedicated hardware for each tomographic modality.

Cui et al. (2009) reported the construction of a tomographic sensor integrating in the same plane ERT and ECT sensors. The sensor construction is performed by the placement of metallic plates around the pipe. This metallic plates perform the role of capacitive electrodes. The authors report the possibility for the capacitance measurements to be performed with either internal or external capacitive electrodes. Thus, it can be chosen whether the ECT modality is intrusive or not. The resistive electrodes are mounted in the gaps between the capacitive sensors. Due to the need of current flowing through the media in order to perform ERT imaging, the resistive electrodes have to be in contact with the materials inside the sensor. In consequence, the ERT modality is invasive but non-intrusive.

The measurements for each modality are taken in sequence, one modality after other. While taking capacitance measurements, the ERT electrodes are connected to ground, performing the function of radial grounded guards. Once all the capacitance measurements are gathered, the system changes to ERT modality and the ECT electrodes are floated while conductance measurements are taken.

This type of construction has the advantage of integrating both tomographic sensors in the same axial plane, allowing to get the conductivity and permittivity distributions in the same space. Some drawbacks of this system are the difficulty of the sensor construction, the need of two measurement systems, one for each modality.

The following are some systems in the category of dual modality tomographic system performing capacitance and conductance measurements over the same electrodes.

Li and Yang (2009) reported a system able to measure both characteristics, conductivity and capacitance simultaneously with the use of a single ECT sensor with internal

electrodes. This system is based on an impedance analyser to perform the measurements. Image reconstruction is performed separately and afterwards image fusion is used to get a representation of the information gotten by both modalities. The advantages of this system are, the possibility of taking both measurements simultaneously in the same axial plane, and the ease of the sensor construction. A drawback of this system is its dependency of an impedance analyser.

Cao at al. (2010) reported the construction of a tomographic system with an external electrodes ECT sensor. The authors describe the process to generate sensitivity maps and image conductive materials by means of the complex admittance. The measurements are performed by the use of a switching unit and an impedance analyser. Some advantages of this system are the simplicity of the sensor and the ease of construction. Additionally, the proposed imaging technique is non-invasive and non-intrusive. A drawback for this technique is its dependence of an impedance analyser to perform the measurements.

Marashdeh et al. (2007) proposed a dual modality system. It consists of the use of an ECT sensor with external electrodes to perform conductivity and capacitance measurements. The determination of the conductivity is based on the measurement of the power dissipated due to the conductive materials. Some advantages of this system are the simplicity of the sensor and the ease of construction. Additionally, the proposed imaging technique is non-invasive and non-intrusive.

Chapter 3

Voltage driven ERT system. Hardware design

3.1 Sensing strategy

In ERT featuring voltage-excitation and current-measurement the sensing strategy is highly similar to ECT. One sensor is set as driving electrode by applying a AC voltage to it. The remaining electrodes are set as sensing electrodes by connecting them to virtual ground on the detecting circuit.
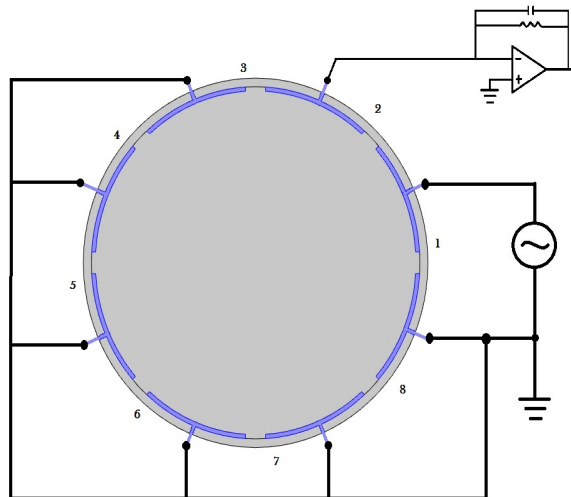
Figure 3.1: 1-2 electrodes measurement.

In addition, the number of independent measurements for ERT with voltage-excitation in defined by the same relation as ECT. The relationship between the number of independent measurements M and the number of electrodes N is given by:

$$M = \frac{N(N-1)}{2} \tag{3.1}$$

From equation 3.1, the number of possible independent measurements M in this modality with a N number of 8 electrodes is 28.

Table 3.1 shows the measurement sequence for an ERT sensor featuring a voltage-excitation and current-measurement scheme. As can be seen by table 2.1 in section 2.2.1, the measurement sequence is indeed the same for ECT and ERT sensors with the same number of electrodes. In the sequence depicted in table 3.1 the number of elec-trodes is 8. In every cell shown in this table there is a piar of numbers. For example, in the first cell on the far left side column there is an 1-2. This means that the mea-surement number 1 is taken between the electrode number 1, performing as driving electrode, and the electrode number 2, performing as detecting electrode. After this measurement is taken, the sensing electrode is changed and the current value is mea-sured in between elecrtodes 1 and 3. This sequence continues until all the independent measurements are gathered. This is, until the measurement shown in the cell in the far right side of the table is taken, the 28th measurement corresponds to the value of the current flowing from electrode 7 to electrode 8.

1-2	2-3	3-4	4-5	5-6	6-7	7-8
1-3	2-4	3-5	4-6	5-7	6-8	
1-4	2-5	3-6	4-7	5-8		
1-5	2-6	3-7	4-8			
1-6	2-7	3-8				
1-7	2-8					
1-8						

Table 3.1: Measurement sequence for an 8 electrodes ERT sensor with voltage excita-tion and current measurement

3.2   Sensor design

ERT requires the flow of current through the material in order to detect conductivity changes and gather enough information to perform image reconstruction. This requires the construction of a tomographic sensor with internal electrodes. The electrodes are fixed in the inner face of a pipe or vessel wall. A metallic screw passes through the pipe wall and it performs two tasks, the first one is to hold the electrodes in their position and the second is to allow the electrical connection between the circuitry and

the electrodes placed inside the container. As can be seen, the construction of a sensor for ERT with voltage excitation does not differ with the construction of an ECT sensor with inner electrodes.
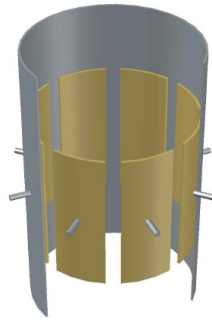
Figure 3.2: ERT with voltage excitation, sensor construction.

In ECT sensors is usual the use of a grounded ring in both axial ends of the electrodes to reduce the noise and fringe effect (Xu et al., 1999). In the application of ERT with voltage excitation the use of a grounded ring on each axial electrode end would help to reduce noise. The difficulty of constructing an internal grounded ring and the drain of current form the driving electrode into the grounded rings are the main reasons to locate the axial ends on the external face of the pipe wall.
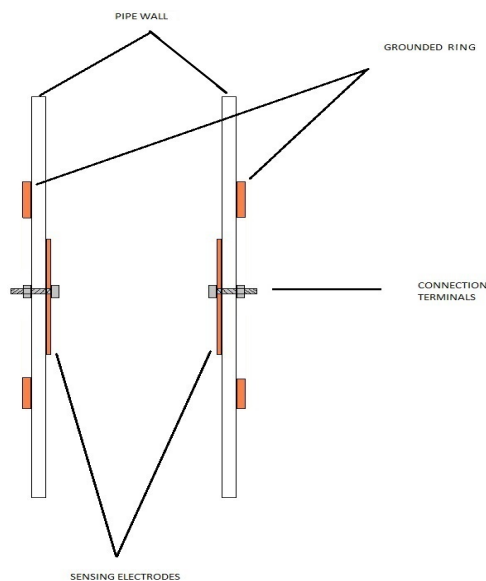
Figure 3.3: ERT sensor with grounded rings.

In Figure 3.3 it is possible to see the construction of an ERT sensor with grounded rings at both axial ends.

The parameters of the built sensor are the following:

- Number of electrodes *N*=8

- Electrode axial length 6.5 cm

- Electrode Radial length 2.1 cm

- Inter electrode radial gap 1 cm

- Earthed ring axial length 2 cm

- Axial distance between electrodes and grounded ring .5 cm

- Container diameter 7.3 cm

- Thickness of container's wall .3 cm

ERT sensor with driven guards

(a) Full view   (b) Cut view
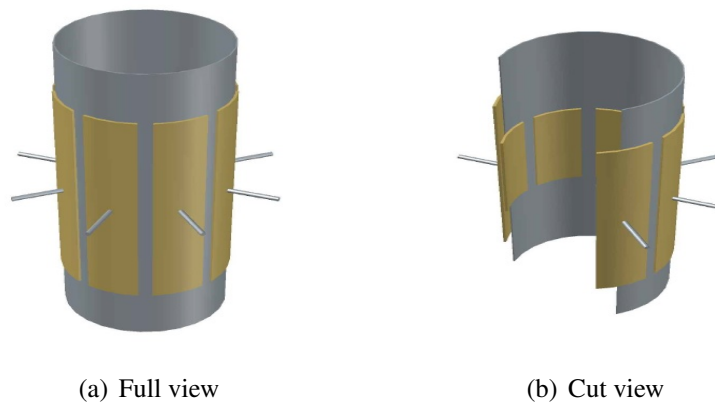
Figure 3.4: ERT with voltage excitation, sensor construction with external driven guards.

The construction of a sensor with driven guards for ERT with voltage-excitation is quite similar to a standard ECT sensor with inner electrodes. The only change is the location of metallic plates in the outer face of the container wall. These metallic plates are mechanically fixed and electrically connected to the inner electrodes by the screws passing through the container's wall. The axial size for the driven guards is larger than

the size of the internal electrodes, extending beyond the axial end of the electrodes in both directions. The radial size of the driven guards and the internal electrodes is the same.
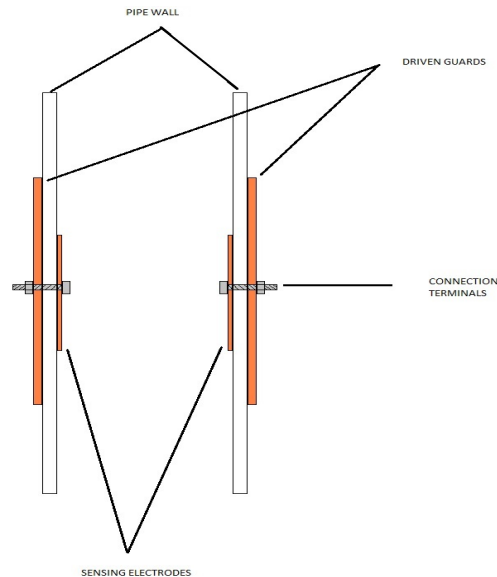
Figure 3.5: ERT sensor with external driven guards.

The parameters of the built sensor are the following:

- Number of electrodes *N*=8

- Electrode axial length: 6 cm

- Electrode Radial length: 2.1 cm

- Inter electrode radial gap: .5 cm

- Driven guard axial length: 10 cm

- Driven guard radial length: 2.1 cm

- Container diameter: 7 cm

- Thickness of container's wall: .1 cm

- Screw length and diameter: .7 cm and .2 cm

The driven guards in this modality of ERT have the task of building an electric field inside the pipe wall, generation a more homogeneous electric field in the axial direction.

In consequence, a reduction in the fringe effect is expected. Additionally, these driven guards are mounted in the outer face of the container's wall. This means they are not in contact with the materials inside the sensor. As a result, the wall acts as an electrical insulator avoiding the electric current to flow from the driven guards into the area to be imaged, preventing in this way disturbances in the conductance measurements.

3.3   Agilent 34972A-based ERT imaging system

In this work, an Agilent 34972A unit is used to perform the switching control and data acquisition. The device has a built in digital multimeter to perform the measurement of the VRMS voltage . In addition, this DAQ unit allows the use of up to three interchangeable cards to configure the system with different inputs. The cards used to this system set-up are:

- Agilent 34903A card

  20-channel general porpoise switch card. It is built with single pole, double throw latching relays. Electrical specifications: 300 V, 1 A, 10 MHz bandwidth. These switches are only for control or actuator driving, therefore there is not connection to the internal digital multimeter.

- Agilent 34902A card

  16-channel High-speed multiplexer. This multiplexer card is built with reed relays allowing up to 250 ch/s scanning. Electrical specifications: 300 V, 50 mA, 10 MHz bandwidth. These switches are used for multiplexing signals to perform the measurement with the internal digital multimeter.

For this system set-up, the above mentioned cards were used, the card 34903A was used to perform the switching. This is to change the electrode's modality between driving and sensing electrode. For an ERT system with 8 electrodes sensor, 14 channels were used.

One channel from the card 34902A was used to connect the current to voltage converter circuit to the digital multimeter built-in in the DAQ system.

Figure 3.6 shows the diagram of the system built for the data acquisition stage. In an idle stage, all the electrodes are connected to ground. When a measurement cycle begins, the switches are activated following the sequence depicted in table 3.2. In this

table, there is a column describing the switch combination for each of the possible 28 measurements available with an 8 electrodes ERT sensor.

To illustrate the change of modality, the first measurement, in order to set electrode number 1 as driving electrode the switch J1 is activated, connecting in this way the electrode number one directly to the AC voltage source. On the other hand, to set electrode number 2 as sensing electrode, switches J2 and J9 are activated, connecting in this way the electrode number 2 to the inverting terminal on the current to voltage converter. In consequence, a voltage proportional to the current flowing from electrode 1 to electrode 2 can be measured with the digital multimeter and recorded to later perform image reconstruction. This switching sequence continues until all the 28 possible measurements are gathered.

	1	2	3	4	5	6	7	8	9	10	11	12	13	14	15	16	17	18	19	20	21	22	23	24	25	26	27	28
J1	ON	ON	ON	ON	ON	ON	ON	-	-	-	-	-	-	-	-	-	-	-	-	-	-	-	-	-	-	-	-	-
J2	ON	-	-	-	-	-	-	ON	ON	ON	ON	ON	ON	-	-	-	-	-	-	-	-	-	-	-	-	-	-	-
J3	-	ON	-	-	-	-	-	ON	-	-	-	-	-	ON	ON	ON	ON	ON	-	-	-	-	-	-	-	-	-	-
J4	-	-	ON	-	-	-	-	-	ON	-	-	-	-	ON	-	-	-	-	ON	ON	ON	ON	-	-	-	-	-	-
J5	-	-	-	ON	-	-	-	-	-	ON	-	-	-	-	ON	-	-	-	ON	-	-	-	ON	ON	ON	-	-	-
J6	-	-	-	-	ON	-	-	-	-	-	ON	-	-	-	-	ON	-	-	-	ON	-	-	ON	-	-	ON	ON	-
J7	-	-	-	-	-	ON	-	-	-	-	-	ON	-	-	-	-	ON	-	-	-	ON	-	-	ON	-	ON	-	ON
J8	-	-	-	-	-	-	ON	-	-	-	-	-	ON	-	-	-	-	ON	-	-	-	ON	-	-	ON	-	ON	ON
J9	ON	-	-	-	-	-	-	-	-	-	-	-	-	-	-	-	-	-	-	-	-	-	-	-	-	-	-	-
J10	-	ON	-	-	-	-	-	ON	-	-	-	-	-	-	-	-	-	-	-	-	-	-	-	-	-	-	-	-
J11	-	-	ON	-	-	-	-	-	ON	-	-	-	-	ON	-	-	-	-	-	-	-	-	-	-	-	-	-	-
J12	-	-	-	ON	-	-	-	-	-	ON	-	-	-	-	ON	-	-	-	ON	-	-	-	-	-	-	-	-	-
J13	-	-	-	-	ON	-	-	-	-	-	ON	-	-	-	-	ON	-	-	-	ON	-	-	ON	-	-	-	-	-
J14	-	-	-	-	-	ON	-	-	-	-	-	ON	-	-	-	-	ON	-	-	-	ON	-	-	ON	-	ON	-	ON

Table 3.2: Switch sequence

The DAQ Agilent 34972A has a built-in LAN card, allowing to stablish a fast PC-DAQ communication channel. The switching control and data acquisition is made with a graphic user interface through a web browser. Figure 3.7 shows the graphic interface in which all the switches can be controlled manually by clicking over the image representing the switch to be activated. In addition, the interface shows the current state of all the switches to allow better control of the switching sequence.

Once all the measurements are gathered, a .txt file is generated from the graphic interface. Such file contains the desired VRMS measurements and is stored in the PC's hard drive to later perform image reconstruction.
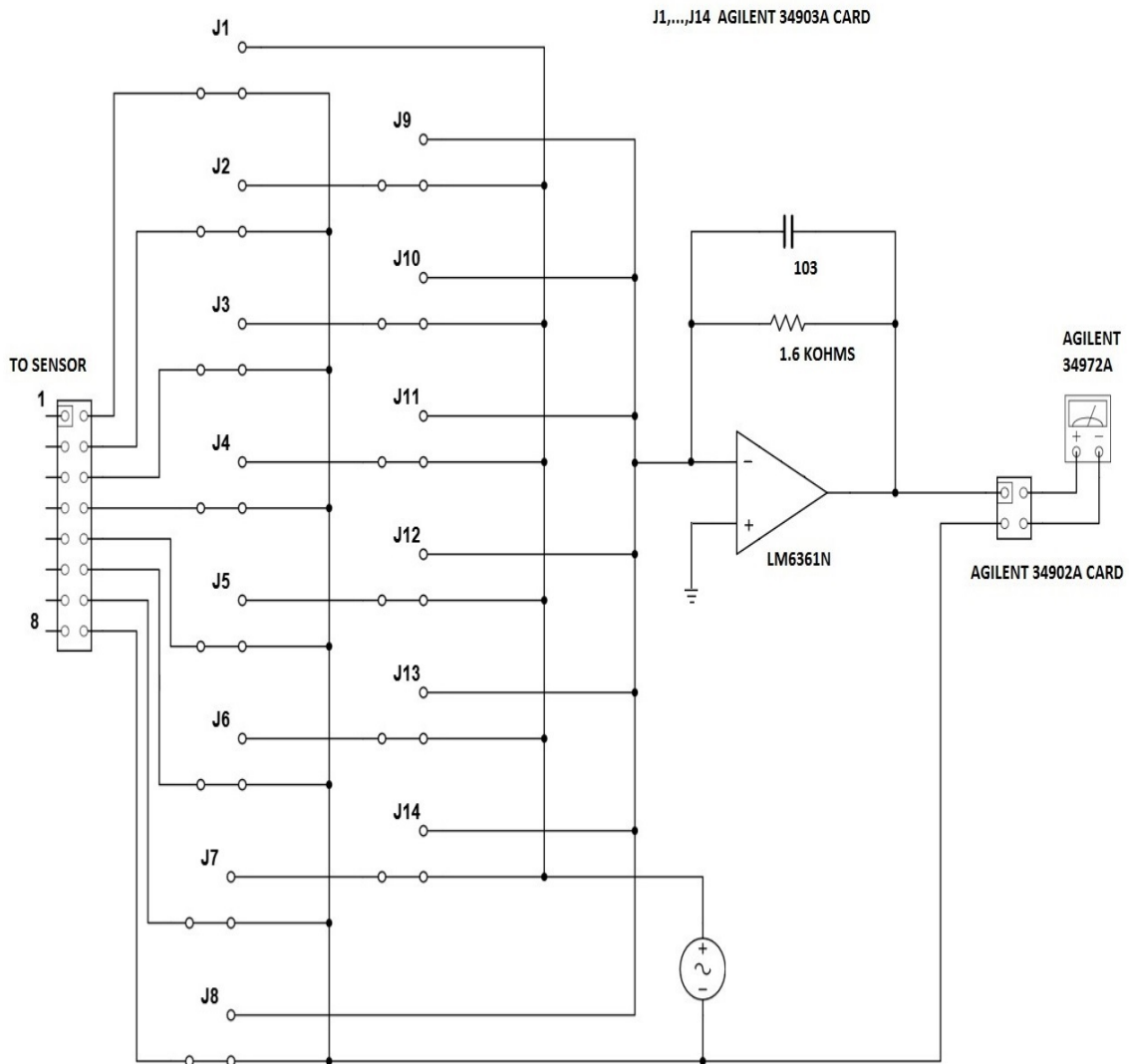
Figure 3.6: Switching and sensing circuit.
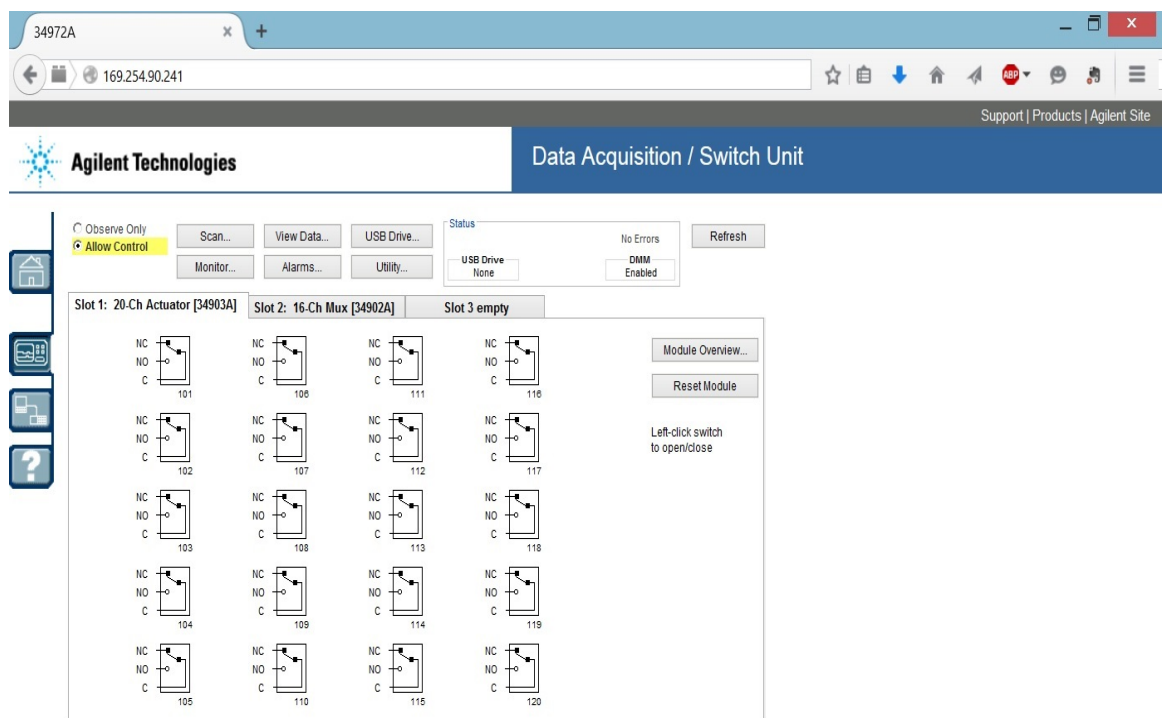
Figure 3.7: Agilent user interface.

Voltage source

A TG315 function generator was the device on charge to generate the sine AC voltage fed to the system. During the test, a variety of different frequencies and voltages were tested to get the best performance. The main characteristics of such function generator are the following:

- Frequency range: .003 Hz to 3.179 MHz

- Voltage output: .4 mVrms to 5.9 Vrms

- Waveforms available: Sine, square and triangular.

- Output impedance: 600 Ω and 50 Ω

- DC offset: from 10 to -10 DCV

- Auxiliary output: TTL

3.3.1   Current to voltage converter

In ERT with voltage excitation and current measurement, it is necessary the quantify the amount of current flowing from the driving electrode to all the sensing electrodes. In this system set-up, a single transimpedance amplifier with a fixed gain is used to perform this task.
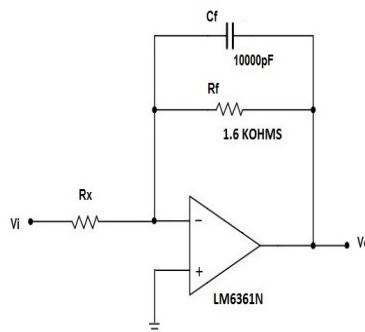
Figure 3.8: Transimpedance amplifier

The relationship between the current input and the output voltage can be described by

$$Vo = -\frac{Z_f}{R_x}Vi \qquad\qquad (3.2)$$

where $Zf = \dfrac{R_f}{j\omega C_f R_f + 1}$ and Vi is the voltage applied to the sensor.

3.3.2 Operating frequency

Considering the phenomenon inside the sensor as a parallel arrangement of resistive and capacitive impedances, it is possible to minimize the effect of the capacitive impedance over the measured current. From Equation 3.3, it can be seen that setting a low operating frequency generates an increase in the capacitive impedance. Whereas form Equation 3.4 the resistive impedance is not a function of the frequency. In consequence, if setting a low operating frequency the resistive component in the parallel arrangement of impedances is smaller in magnitude than the capacitive. Therefore, the measured current is only a function of the resistive impedance.

The capacitive impedance is represented by:

$$Z_c = \frac{1}{j\omega C} \tag{3.3}$$

The resistive impedance can be determined by:

$$Z_r = R \tag{3.4}$$

The inductive impedance can be obtained form:

$$Z_i = j\omega L \tag{3.5}$$

The phase change between voltage and current due to the capacitive and resistive characteristics of the media to be imaged can be measured to determine the operating frequency. The current due to a mainly resistive impedance is always in phase with the voltage applied to it. In contrast, the current flowing trough a mainly capacitive impedance shows a phase angle change of 90 degrees respect to the voltage on such impedance. In this way, by using an oscilloscope, it is possible to monitor the phase angle and assure that the measured current is only a function of the resistive impedance.

The system built in this work is devised to be capable to image conductive materials within a range of .01 $\dfrac{S}{m}$, that is the common conductivity of tap water. To 5 $\dfrac{S}{m}$, that is

the common conductivity of sea water.

Table 3.3 shows a set of phase angle measurements while having the sensor filled with water with a conductivity of .01 $\frac{S}{m}$. It is possible to see the reduction of the phase angle as the excitation frequency is decreased.

	Phase angle (°)	
Frequency	Adjacent electrodes	Opposite electrodes
100 kHz	13	10
50 kHz	9	6
20 kHz	5	3
10 kHz	2	1
5 kHz	0	0

Table 3.3: Phase angle in function of frequency. Sensor filled with water with a conductivity of .01 $\frac{S}{m}$

As the conductivity of the water increases, the resistive impedance decreases and the capacitive effect seen in the measured current is reduced. In experiment the rise of the water's conductivity is done by adding salt to emulate sea water.

Table 3.4 shows a set of phase angle measurements while having the sensor filled with water with a conductivity of 5 $\frac{S}{m}$.

	Phase angle (°)	
Frequency	Adjacent electrodes	Opposite electrodes
100 kHz	22	16
50 kHz	10	8
20 kHz	2	0
10 kHz	0	0
5 kHz	-6	-5

Table 3.4: Phase angle in function of frequency. Sensor filled with water with a conductivity of 5 $\frac{S}{m}$

From the latter, if the operating frequency is set at 10 kHz or below, the capacitive effects can be neglected and the voltage output of the transimpedace amplifier is only function of the material's resistive property. On the other hand, form Equation 3.5, the inductive impedance decreases alongside with the frequency, therefore, the operating frequency cannot be reduced unlimitedly. As it can be seen from table 3.4, due to the short distance and high conductivity of the saline solution, when decreasing the

frequency below 10 kHz, an inductive effect can be seen in the measured current. In conclusion, the operating frequency to image only the material's resistive characteristic on the selected range of conductivities is 10 kHz.

Chapter 4

Image Reconstruction

4.1 Forward problem

The forward problem in ERT with voltage-excitation and current-detection consists in the determination of the current values in the boundaries due to a given conductivity distribution.

The phenomenon inside the sensor's area can be described by the use of the Poisson's equation. Equation 2.5 is used with Dirichlet boundary conditions $\phi = Vi$ in the driving electrode and $\phi = 0V$ in the remaining electrodes.

4.1.1 Sensitivity map generation

The generation of the sensitivity maps in this work was performed by two different methods.

First, by the procedure described in section sensitivity maps in 2.2.3. This method consists of the determination of the sensibility between two given electrodes by performing the dot product between the electric fields generated by each electrode when the driving voltage is applied to them once at the time.

28 sensitivity maps are calculated in MATLAB by applying equation 2.7. The flow chart in Figure 4.1 describes the process of sensitivity map generation. The complete code can be found in appendix B.

The process makes use of N .txt files. N being the number of electrodes. Each file contains the potential distribution due to a electrode set to the driving voltage and the rest of electrodes set to 0V. The data is exported from COMSOL and is arranged in two columns, the first one containing the X,Y coordinates and the second the voltage at such position.
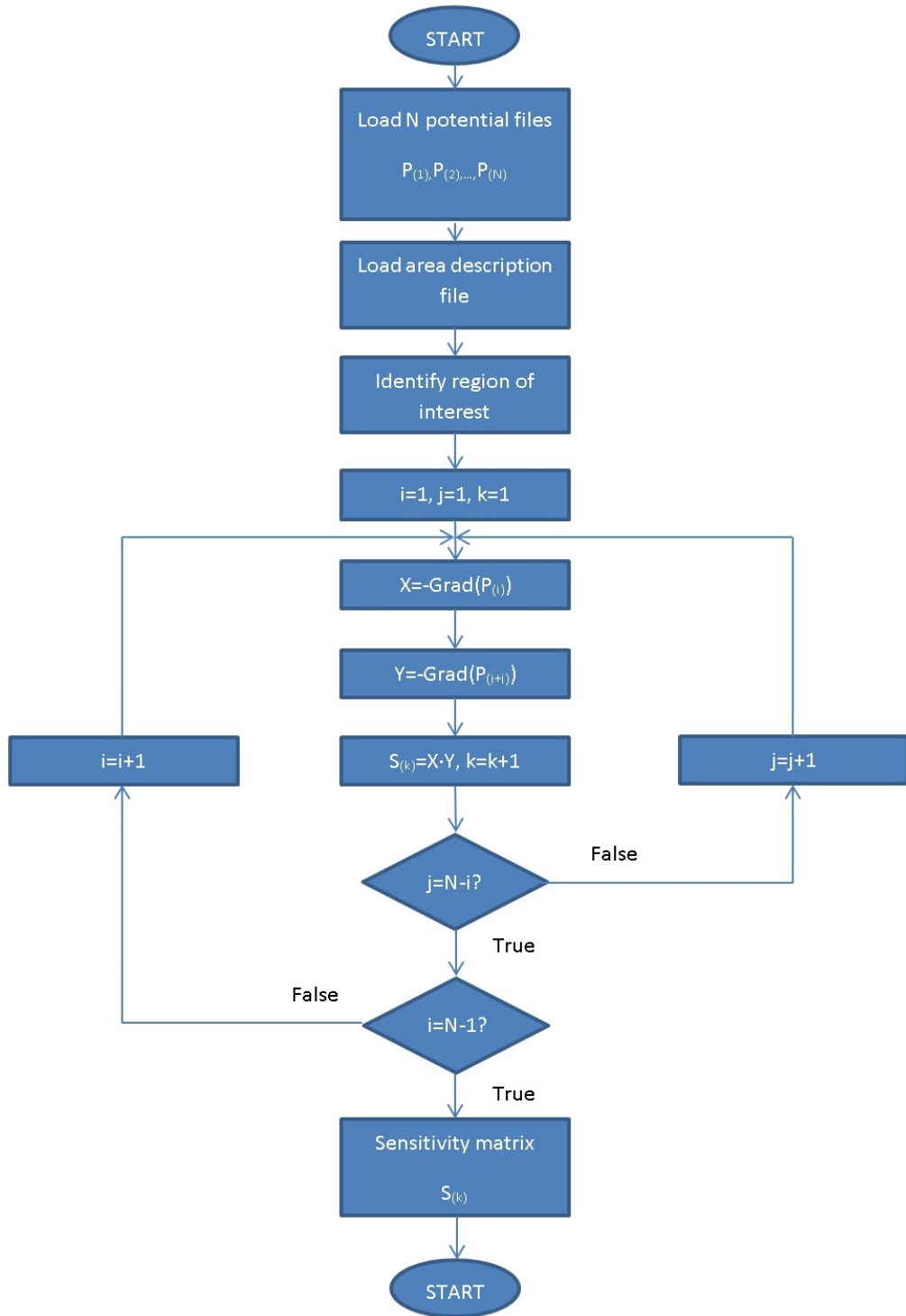
Figure 4.1: Sensitivity map generation

Table 4.1 shows the sensitivity maps for adjacent and opposite electrode pairs. Such sensitivity maps were generated with the latter described procedure. The sensitivity maps were generated applying an AC excitation voltage with a frequencies of 10kHz. Due to the symmetry of the sensor, it is possible to calculate only the first seven sensitivity maps for an 8 electrode sensor and rotate them to complete the full set of sensitivity maps. A set of the first 7 sensitivity maps can be found in Appendix E.

The characteristics of the model are the following:

- Number of electrodes: 8

- Sensor diameter: 7 cm

- Excitation voltage: .1VRMS

- Excitation frequency: 10kHz

- Boundary conditions: Electric potential in the driving electrode, Ground in the Sensing electrodes. Electrical insulation in the rest of boundaries.

Adjacent electrode pair
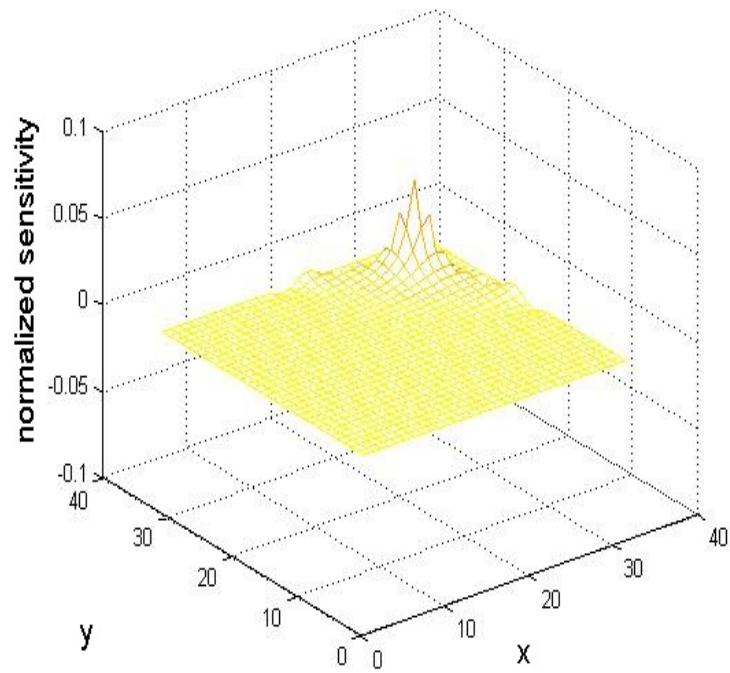
Opposite electrode pair
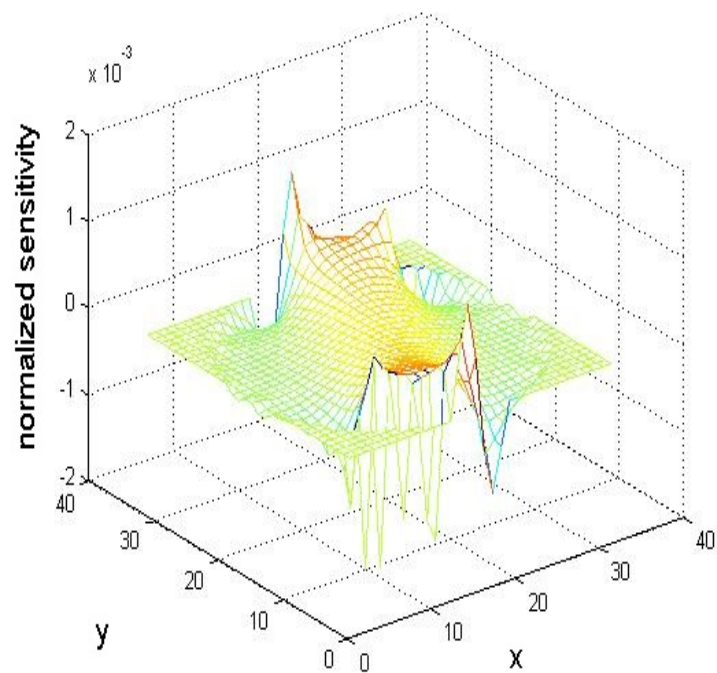
Table 4.1: Sensitivity maps calculated from electric fields

The second method consists of measuring the response of a CAD version of the sensor using COMSOL. Making use of the connection capabilities between such FEM software and MATLAB, a script has been develop to measure the response of the system to a small perturbation placed inside the sensor filled with conductive material.

Once the COMSOL model is built, a square grid is constructed within the sensing area in the model. The size of such square area is defined by the desired resolution, in this case 32x32 pixels. In consequence the pixel's size is .21875 cm. Figure 4.2 shows the COMSOL model used to calculate the sensitivity maps. The conductivity of the background material is set to 1 S/cm. Therefore, it is defined as conductive media. In addition, the conductivity of the material inside the pixel acting as a test probe is set to 2 S/cm. Afterwards, the electrode number one is set as driving electrode and the system is solved to obtain the current on the remaining electrodes. Once the system's response is stored in a matrix, the conductivity of the material inside the next pixel is changed and the system is solved once more. This process is repeated until the system's response is recorded for all the pixels in the grid have been set as test probe with high conductivity material. Once the process is completed, the electrode number two is set a driving electrode and the procedure is repeated until all the measurements have been gathered.
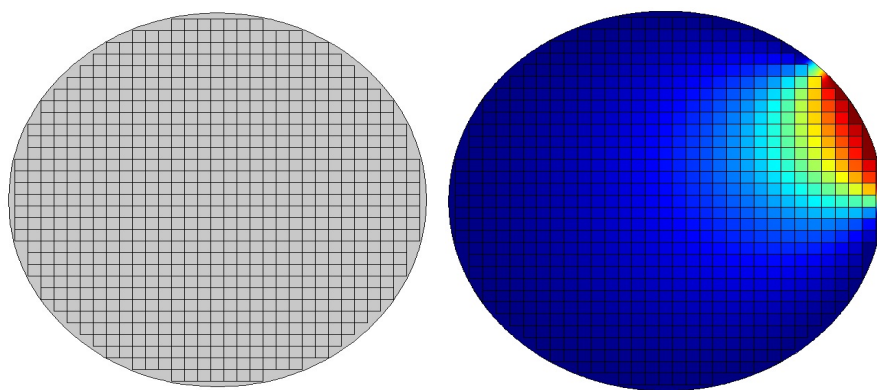
Figure 4.2: COMSOL model with testing grid.

The characteristics of the COMSOL model are the following:

- Number of electrodes: 8

- Sensor diameter: 7 cm

- Excitation voltage: 1V

- Excitation frequency: 10kHz

- Boundary conditions: Electric potential in the driving electrode, Ground in the Sensing electrodes. Electrical insulation in the rest of boundaries.

Figure 4.3 shows a flow chart describing the procedure of sensitivity maps generation. The complete script can be found in Appendix A.

Due that the forward problem has to be solved repeatedly, this procedure is time consuming and requires a substantial computing power. On the other hand, the main advantage of this approach is that the obtained sensitivity map is the closest approximation to the real sensor's sensitivity. This is also useful to confirm the sensitivity maps obtained by other procedures.

Table 4.2 shows the sensitivity maps for adjacent and opposite electrode pairs calculated form the COMSOL model. Due to the circular symmetry of the sensor, it is possible to calculate only the first seven sensitivity maps for an 8 electrode sensor and rotate them to complete the full set of sensitivity maps. A set of the first 7 sensitivity maps can be found in Appendix D.

```
┌─────────────────────┐
│ Load COMSOL model   │
│    to MATLAB        │
└─────────────────────┘
          │
┌─────────────────────┐
│ Define segment lines│
│   for each electrode│
│      elec_(a,:)     │
│      a=1,2,..,N      │
│ N number of electrodes
└─────────────────────┘
          │
┌─────────────────────┐
│       i=1, j=1      │
│ set coordinate vector│
│      C(1:1024)      │
└─────────────────────┘
          │
┌─────────────────────┐
│ Set all electrodes to│
│       ground        │
└─────────────────────┘
          │
┌─────────────────────┐
│ Set elec_(i,:) as   │
│  driving electrode  │
└─────────────────────┘
          │
┌─────────────────────┐        ┌───────────────┐
│ Set all pixels to   │        │   i=i+1, j=0  │
│ low conductivity    │        └───────────────┘
│ Set j pixel to hi   │
│ conductivity        │
└─────────────────────┘
          │
┌─────────────────────┐
│ Solve the system to │
│ obtain current value│
│   in the electrodes │
└─────────────────────┘
          │
┌─────────────────────┐        ┌───────────────┐
│ Measure the current │        │    j=j+1      │
│    in electrodes    │        └───────────────┘
│elec_(i+1,:),...,elec_(N,:)
└─────────────────────┘
          │
┌─────────────────────┐
│ Store current values│
│      in S(j,:)      │
└─────────────────────┘
          │
      ◇ j=1024? ◇
          │
      ◇ i=7? ◇
          │
┌─────────────────────┐
│  Save sensitivity   │
│       maps          │
│        S            │
└─────────────────────┘
```

Figure 4.3: Sensitivity map generation from COMSOL model

Adjacent electrode pair
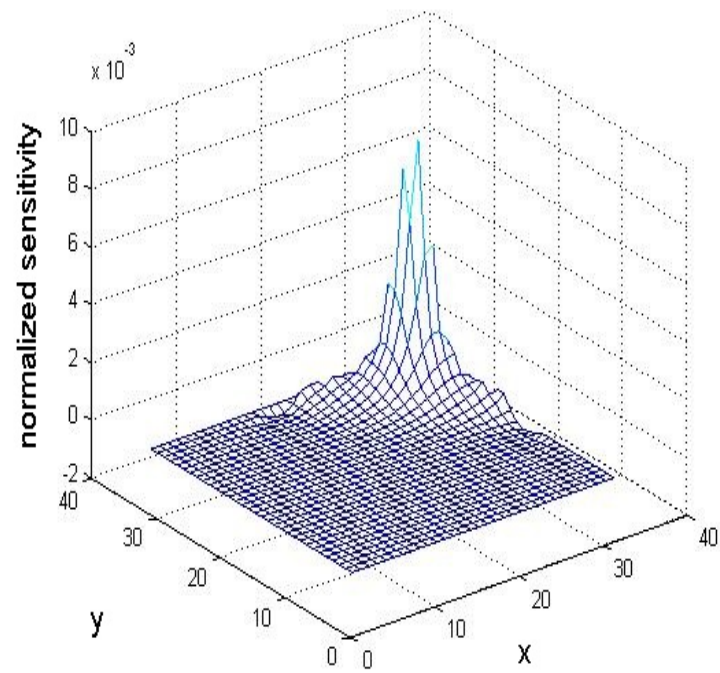
Opposite electrode pair
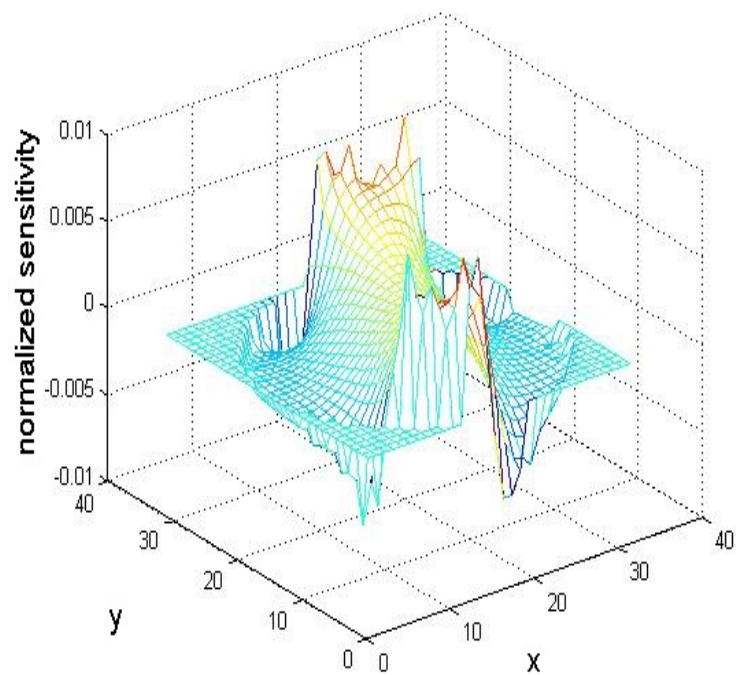
Table 4.2: Sensitivity maps calculated from COMSOL model.

4.2   Inverse problem

The inverse problem in ERT is defined as the determination of the conductivity distribution from the measurements gathered in the sensor's boundary.

4.2.1   Image reconstruction algorithms

During this research, the task of image reconstruction is performed by the use of Linear Back Projection and Landweber algorithms.

Linear back projection algorithm has been used to obtain qualitative information regarding the presence, shape and position of the non-conductive test rods used during this research. LBP algorithm is implemented with equation 2.10 as described in section 2.2.4.

For the task of obtaining images representing quantitative information regarding the area under study the Landweber algorithm has been used. The implementation of the projected Landweber algorithm is done with the use of the equations 2.12 and 2.13 as described in section 2.2.4.

Chapter 5

Results and analysis
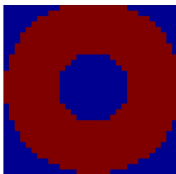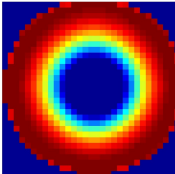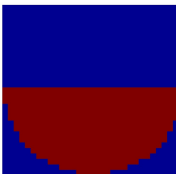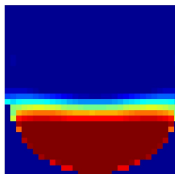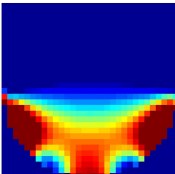
5.1 Image reconstruction
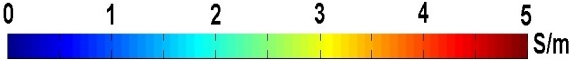
5.1.1 Simulated data from phantoms

In this section, a performance comparison is made between the quality of image reconstruction performed with the sensitivity maps generated with the two techniques described in section 4.1.1. Two phantoms were built to represent central core and stratified flow distributions. Image reconstruction is performed with the LBP and Landweber algorithms. Image error is calculated for each image using (Cao et al., 2009)

$$error = \frac{\| g - g_{ph} \|}{\| g \|} \tag{5.1}$$

Table 5.1 shows the images reconstructed making use of the LBP algorithm. It is possible to see from such table that the image error on qualitative image reconstruction gives similar results with the use of both sensitivity maps. However, the quality of the image from a visual point of view, is clearly superior on these images reconstructed with the use of sensitivity maps generated from the dot product of the electric fields within the sensor.

Phantom	Dot product	Comsol model
Image error (percent)	24	29
Phantom	Dot product	Comsol model
Image error (percent)	47	48

Table 5.1: Image reconstruction LBP algorithm

Table 5.2 and Table 5.3 show image reconstruction of data obtained from a phantom. These set of measurements were reconstructed using the Landweber algorithm. The number of iterations were set at 100 and 400 respectively whereas the relaxation factor was set to 1.2 for both number of iterations.

It is possible to see that the image error decreases for images reconstructed with the sensitivity maps generated with the dot product while the number of iterations increases. With an exception of the image reconstruction of an stratified flow using the sensitivity maps obtained from the COMSOL model.

Table 5.4 and Table 5.5 show image reconstruction using the Landweber algorithm. The number of iterations were set at 100 and 400 whereas the relaxation factor was set at 12.

The increase on the value of the relaxation factor on image reconstruction while using the sensitivity maps from the COMSOL cad allows to reduce the image error for the central core phantom whereas the image reconstruction for the stratified distribution gets distorted and the error increases substantially. On the other hand, image reconstruction for a central core distribution with the dot product sensitivity maps generates a low quality image for a high relaxation factor. Additionally, the increase on the number of iterations decreases further the quality on the reconstructed image for central core. In contrast, for a stratified flow distribution the increase in the relaxation factor

100 iterations, kp=1.2		
Phantom	Dot product	Comsol model
Image error (percent)	19	23
Phantom	Dot product	Comsol model
Image error (percent)	42	47
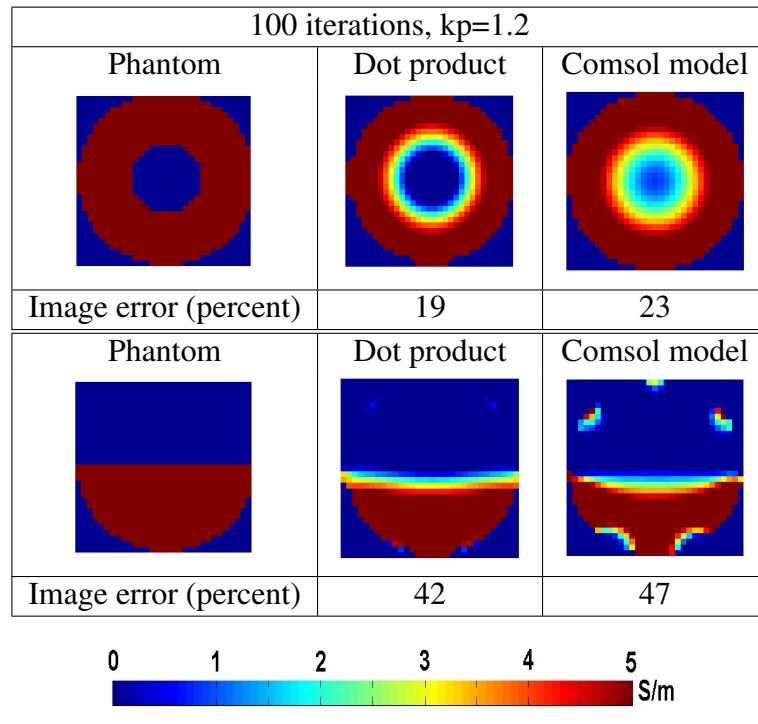
Table 5.2: Image reconstruction Landweber algorithm. 100 iterations kp=1.2

400 iterations, kp=1.2		
Phantom	Dot product	Comsol model
Image error (percent)	18	16
Phantom	Dot product	Comsol model
Image error (percent)	35	55
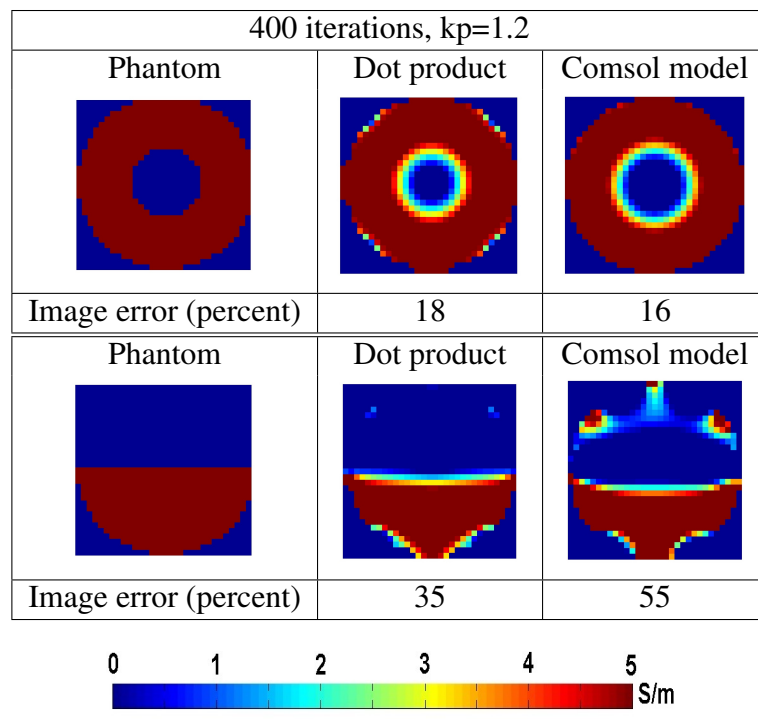
Table 5.3: Image reconstruction Landweber algorithm. kp=1.2

100 iterations, kp=12		
Phantom	Dot product	Comsol model
Image error (percent)	37	15
Phantom	Dot product	Comsol model
Image error (percent)	32	63
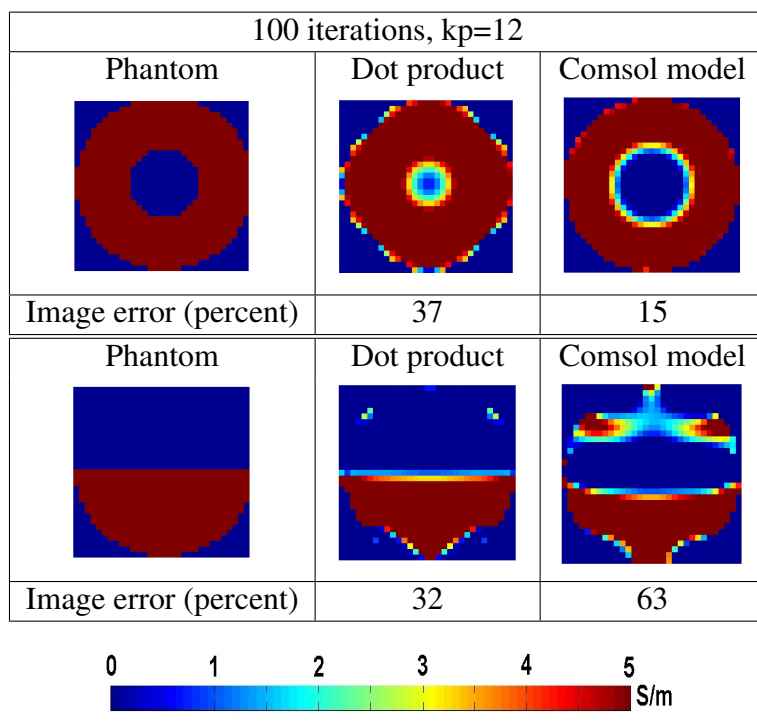
Table 5.4: Image reconstruction Landweber algorithm. 100 iterations kp=12

alongside with a low number of iterations yields a high quality image. The increase on the number of iterations with a large relaxation factor decreases the quality on image reconstruction for such distribution.

400 iterations, kp=12		
Phantom	Dot product	Comsol model
Image error (percent)	51	16
Phantom	Dot product	Comsol model
Image error (percent)	35	72
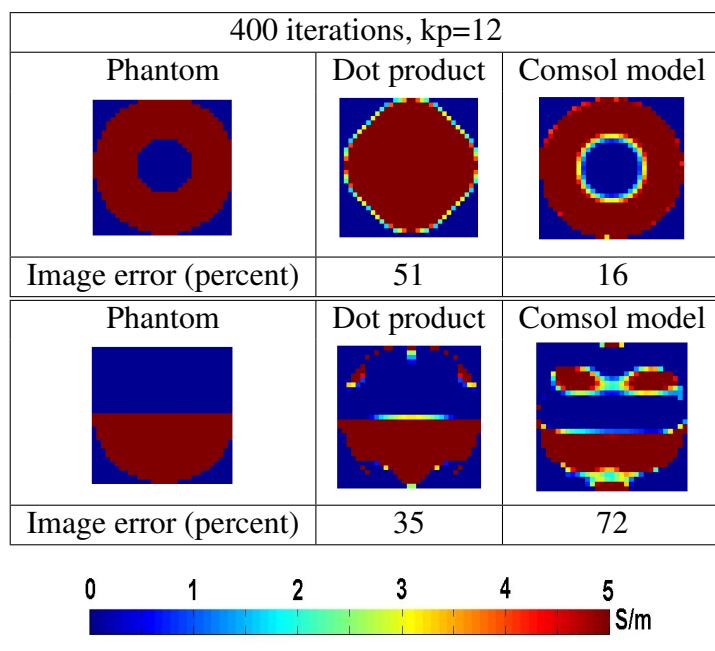
Table 5.5: Image reconstruction Landweber algorithm. 400 iterations kp=12

The results obtained form this comparison let to a trade-off, the images with the highest quality on these set of measurements are those reconstructed with a low number of iterations and a high relaxation factor. The image error for central core distribution is 15 ﹪ when using the sensitivity maps from the COMSOL model. Whereas for a stratified distribution, the image with the lowest error, this is 32 ﹪ is obtained with the use of the sensitivity maps from the dot product between electric fields.

The testing grid built to obtain the sensitivity form the COMSOL model, does not fit the sensor's circular geometry. Therefore, a loss of sensitivity towards the pipe's wall is seen and this causes the distortions seen in image reconstruction for a stratified flow distribution. A major advantage on the use of such sensitivity maps is the quality of the reconstructed image for central core, especially when using a high relaxation factor and low number of iterations with the Landweber algorithm. This generates a image with a reduced error without the need of a high number of iterations. In consequence, image reconstruction is less time and computing power consuming.

5.1.2 Measured data from Agilent system

In this section a set of reconstructed images from measurements taken with the system developed in this work are presented. Image reconstruction is performed with the use of LBP and Ladweber algorithms. The sensor used is the first described in section 3.2, without the use of driven guards.

Central core flow distribution

The experiment consists in the placement of a plastic rod inside the sensor filled with water with a different range of conductivities. The plastic rod is place in the centre of the sensor, allowing in this way to recreate the conditions of a central core flow distribution. Conductivity is controlled by the addition of salt to generate a saline solution emulating sea water. The rod's characteristics are the following:
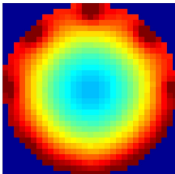
- Diameter: 3 cm

- Length: 21.2 cm

- Material: Perspex

The plastic rod was totally submerged until the bottom of the sensor, 3 cm beyond the end of the electrodes while measurements were taken. Table 5.6 shows the images reconstructed with LBP and Landweber algorithms. The conductivity of the water used in this set of measurements is .01 $\frac{S}{m}$.

Table 5.7 shows the images reconstructed with LBP and Landweber algorithms. Water's conductivity is set at 2.5 $\frac{S}{m}$ thanks to the addition of table salt. Table 5.8 shows the images reconstructed with LBP and Landweber algorithms. Water's conductivity is set at 5 $\frac{S}{m}$, further addition of table salt allows to increase the conductivity, mimicking in this way sea water.

LBP	Landweber kp=1.2	
	100 iterations	200 iterations
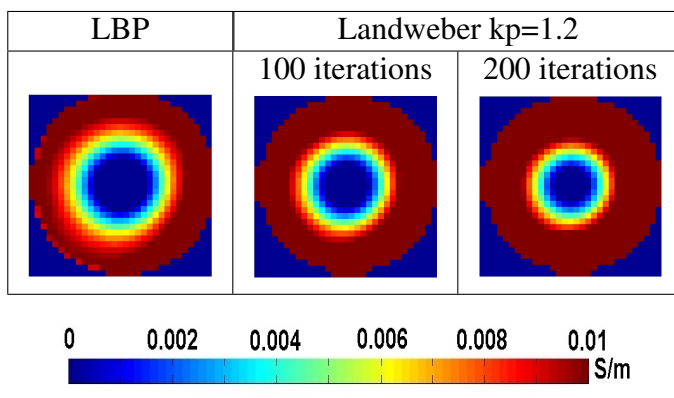
Table 5.6: Image reconstruction plastic rod in water with a conductivity of .01 $\frac{S}{m}$

LBP	Landweber kp=1.2	
	100 iterations	200 iterations
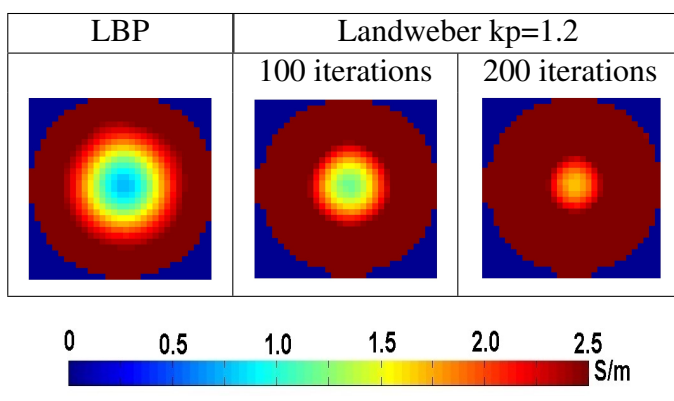
Table 5.7: Image reconstruction plastic rod in water with a conductivity of 2.5 $\frac{S}{m}$

Stratified flow distribution

An experiment was performed to test the system's performance with the presence of an stratified flow distribution. The sensor was half filled with water and put in an
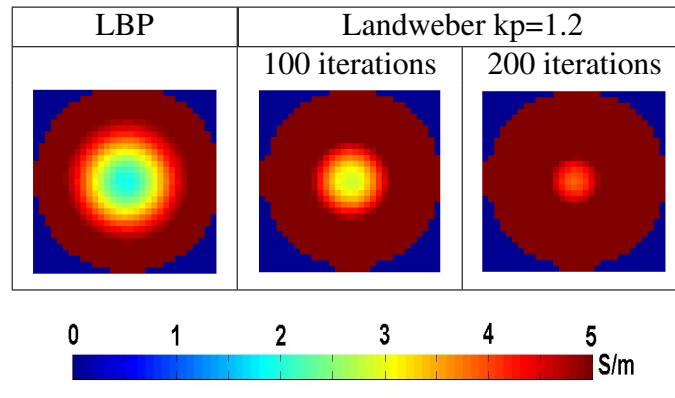
Table 5.8: Image reconstruction plastic rod in water with a conductivity of 5 $\frac{S}{m}$

horizontal position to generate in this way a flow distribution consisting on a half of the sensor filled with water and half of it filled with air.

Table 5.9 shows image reconstruction form measurements taken with water conductivity of .01 $\frac{S}{m}$. Table 5.10 shows image reconstruction form measurements taken with water conductivity of 2.5 $\frac{S}{m}$. Table 5.11 shows image reconstruction form measurements taken with water conductivity of 5 $\frac{S}{m}$
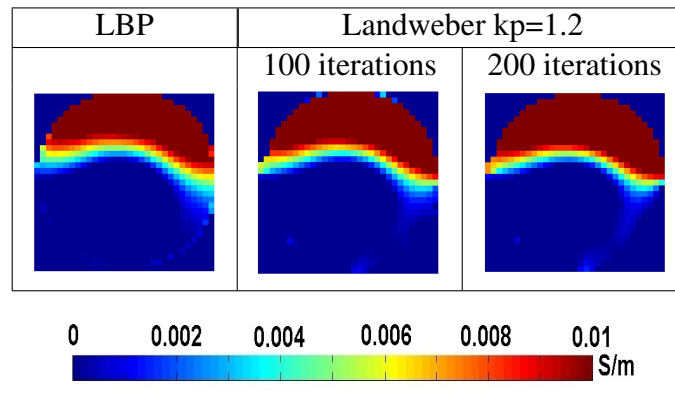
Table 5.9: Image reconstruction stratified flow. Water with a conductivity of .01 $\frac{S}{m}$

As can be seen from the images in Tables 5.9, 5.10 and 5.11, ERT with voltage excitation allows to obtain quality images from complex conductivity distributions like central core and stratified. This is achieved over a wide range of conductivities.

LBP	Landweber kp=1.2	
	100 iterations	200 iterations
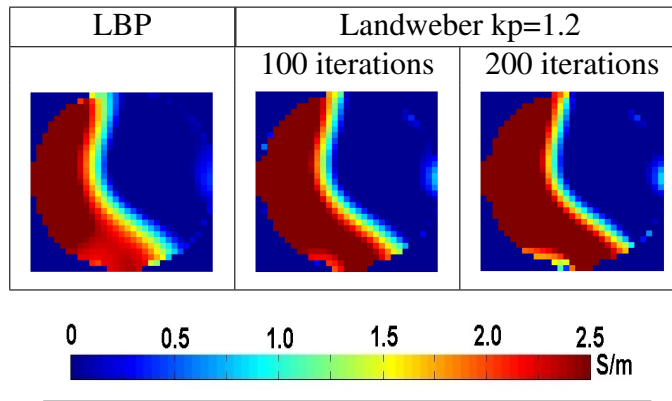
Table 5.10: Image reconstruction stratified flow. Water with a conductivity of 2.5 $\frac{S}{m}$

LBP	Landweber kp=1.2	
	100 iterations	200 iterations
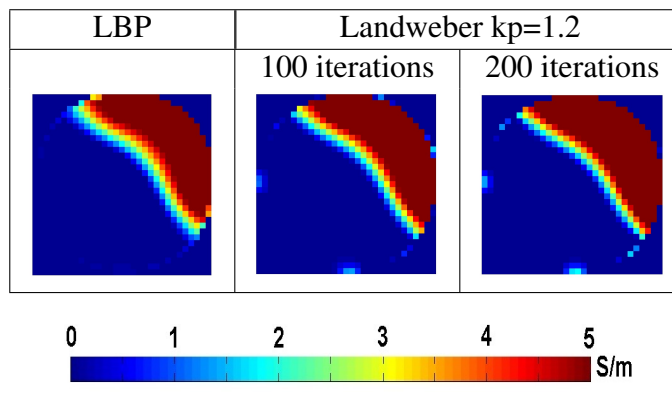
Table 5.11: Image reconstruction stratified flow. Water with a conductivity of 5 $\frac{S}{m}$

5.1.3 Driven guards

In this section, a set of reconstructed images making use of the two types of sensor described in section 3.2. The experiment consists in the placement of a plastic rod inside the sensor filled with water. The plastic rod is placed in different distances relative to the axial centre of the electrodes. The position distance is measured between the axial centre of the sensor electrodes to the tip of the plastic rod that is firstly inserted in the sensor. The conductivity measurements were taken with the use of an impedance analyser based system. Image reconstruction was performed with LBP algorithm and the use of sensitivity maps obtained from the dot product of the electric fields inside the sensor. Table 5.12 shows a set of images reconstructed from data obtained when performing such experiment. The sensor was filled with water with a conductivity of .01 $\frac{S}{m}$. Whereas Table 5.13 shows image reconstruction from the measurements performed over the sensor filled with water with a conductivity of 5 $\frac{S}{m}$.

Position	Driven guards	Earthed ring	Position	Driven guards	Earthed ring
7 cm			1 cm		
6 cm			0 cm		
5 cm			-1 cm		
4 cm			-2 cm		
3 cm			-3 cm		
2 cm			-4 cm		
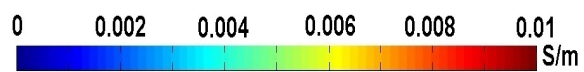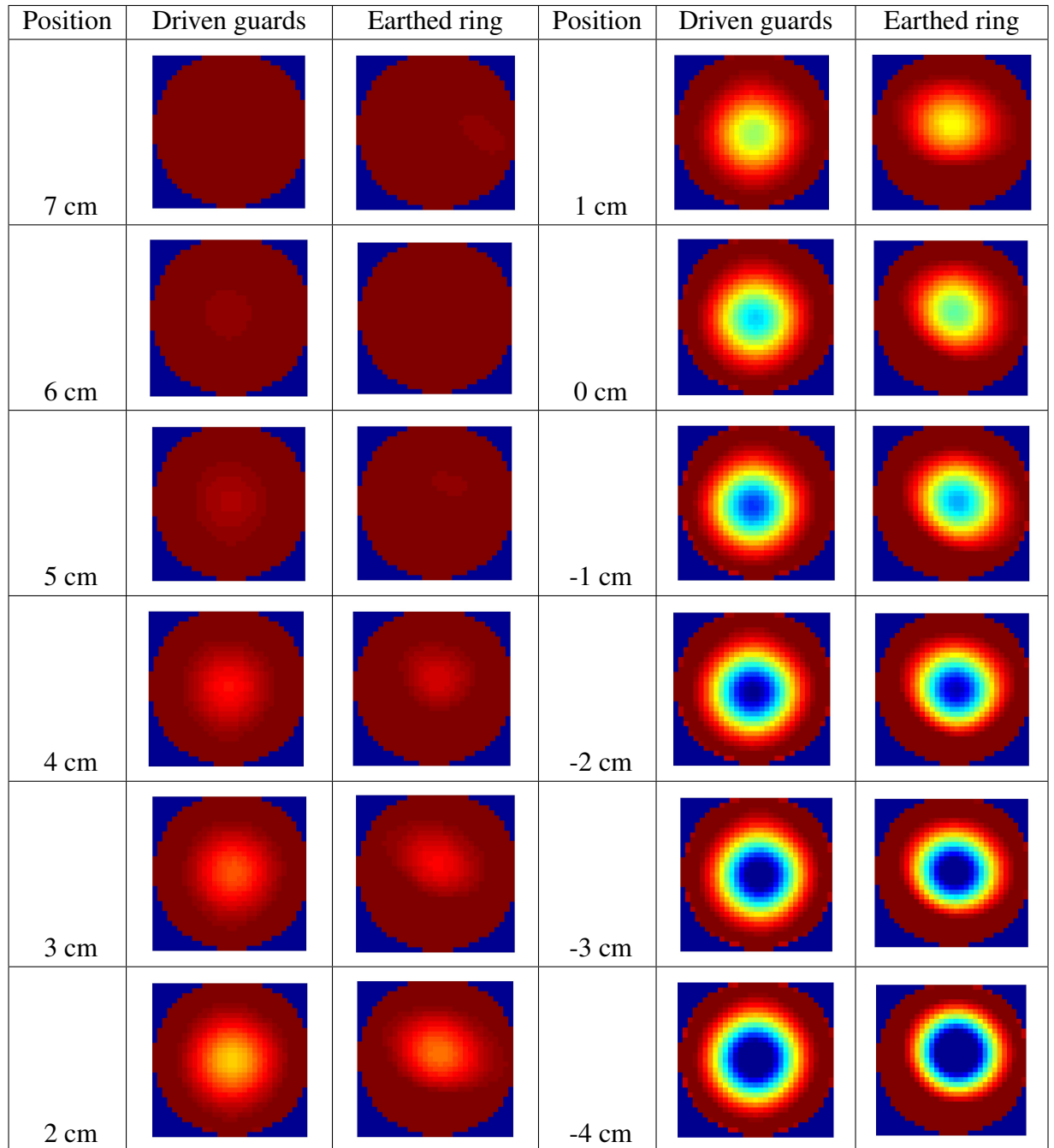
Table 5.12: Water with a conductivity of .01 $\frac{S}{m}$

Position	Driven guards	Earthed ring	Position	Driven guards	Earthed ring
7 cm			1 cm		
6 cm			0 cm		
5 cm			-1 cm		
4 cm			-2 cm		
3 cm			-3 cm		
2 cm			-4 cm		
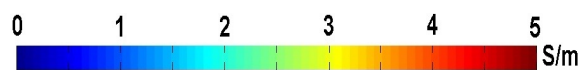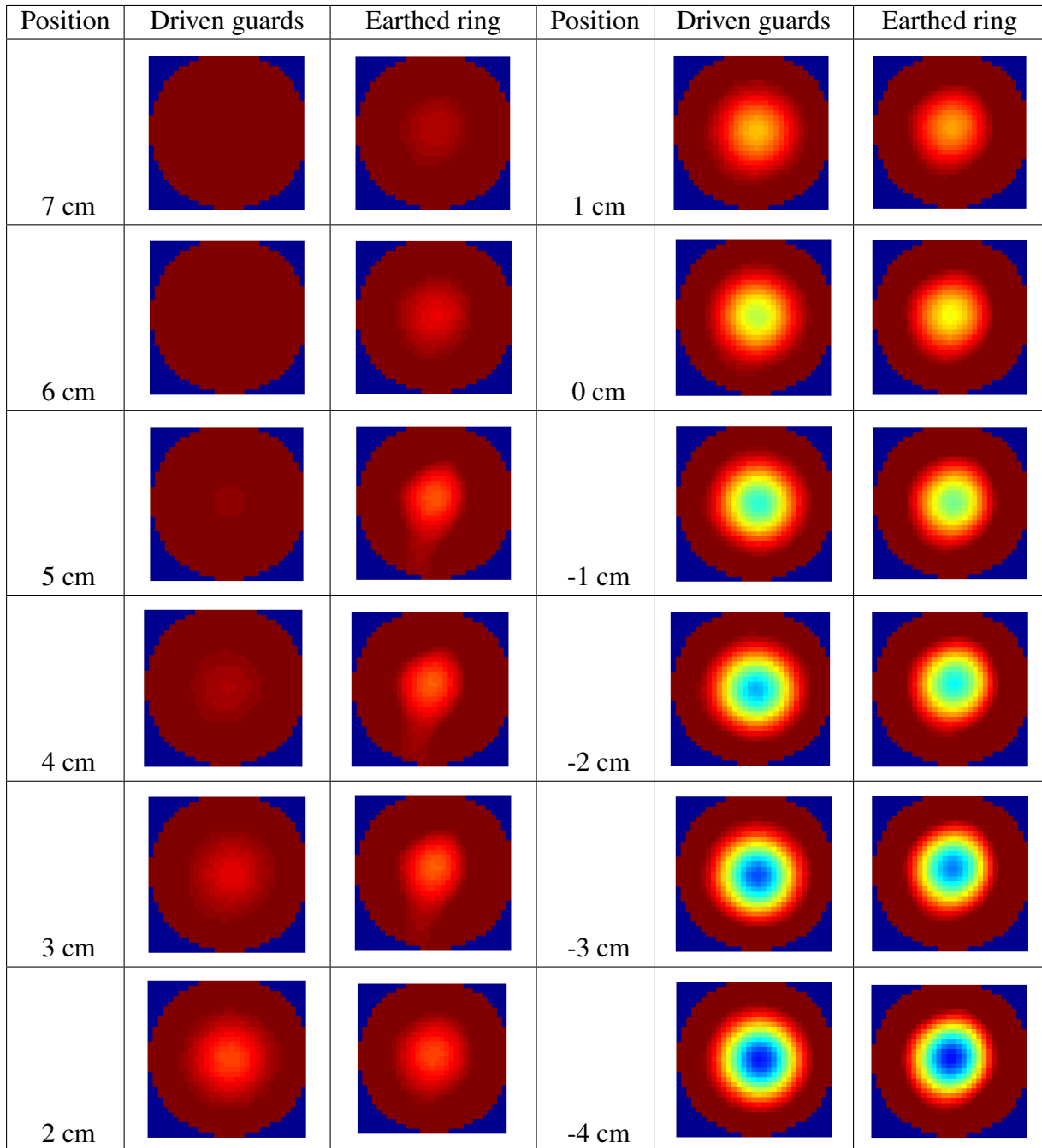
Table 5.13: Water with a conductivity of 5 $\frac{S}{m}$

As can be seen form the images on Tables 5.12 and 5.13, the use of driven guards on ERT with voltage excitation helps to reduce notably the fringe effect. In consequence, there exist a more effective constraint of the sensing field in the axial direction. This can be noticed on the images reconstructed when the plastic rod is over the sensing area. When using a sensor with driven guards, the images do not show the precense of the plastic rod until the distance of the rod's tip and the electrodes is reduced. In addition, it also can be seen how the sensitivity inside the sensing area is increased, when the plastic rod is inside the electrode area, the image is more clear and the shape of the plastic rod is more distinguishable when using driven guards.

5.1.4 Current excitation vs voltage excitation

Further test of the sensor's performance was conducted. This section presents a comparison on performance between ERT with voltage excitation and ERT with current excitation. For ERT with voltage excitation, the sensor with driven guards developed in this work was used, whereas for ERT with current excitation, a sensor was built with small pin electrodes. The characteristics of such sensor are the following:

- Number of electrodes *N*=8

- Electrode diameter: .5 cm

- Inter electrode radial gap: 3 cm

- Container diameter: 7 cm

- Thickness of container's wall: .1 cm

The experiment performed consists in the placement of a plastic rod inside the sensor filled with water with a conductivity of 5 $\frac{S}{m}$. The plastic rod is placed off the centre of the sensor, near to the container's wall whereas in the axial direction it is placed in three different positions, 3 cm over the centre of the electrodes, on the centre of the electrodes and 3 cm below the centre of the electrodes. The characteristics of the plastic rod are the following:

- Diameter: 3 cm

- Length: 21.2 cm

- Material: Perspex

Table 5.14 shows image reconstruction from measurements obtained from the latter described experiment.

Position	Voltage excitation	Current excitation
3 cm		
0 cm		
-3 cm		
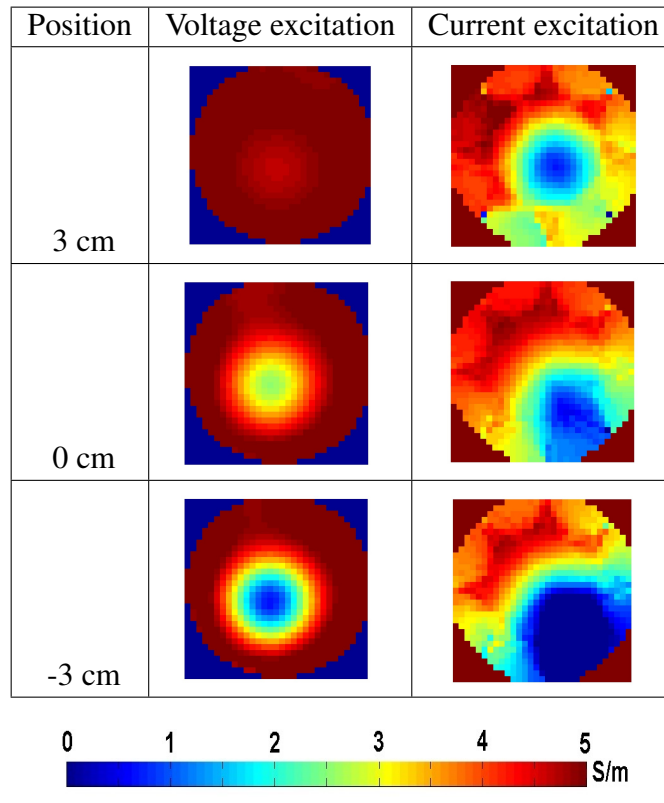
Table 5.14: Performance comparison between ERT with voltage excitation and ERT with current excitation

From image reconstruction obtained form both ERT systems, with voltage and current excitation. It is possible to see the reduction of the fringe effect when using voltage excitation and driven guards. On images obtained with an ERT system with current excitation, the plastic rod is displaced towards the centre of the image when the plastic rod is placed over the sensing plane. This is a well known consequence of the fringe effect. In contrast, on images obtained with ERT featuring voltage excitation, independently of the rod's axial position inside the sensing area, the images show the correct radial position.

Images shown in table 5.14 are visibly of different qualities due that the data on each case has been acquired with ERT systems featuring different SNR and measuring techniques. In addition, the ERT system with voltage excitation allows to get 28 independent measurements whereas the ERT system with current excitation by the use of the adjacent sensing method only allows to gather 20 independent measurements. In consequence, the quality of the reconstructed images from the ERT system with current excitation is significantly lower than those from the ERT system with voltage excitation. Although the quality of the images form the system with current excitation is visibly lower, this comparison is more focused to asses the position of the non-conductive rod inside the region of interest in relation to the real position of the rod rather than the

quality of the reconstructed image. Due to the severe fringe effect seen in ERT with current excitation it is possible to see how the radial position of the plastic rod changes in the reconstructed images when only the axial position of the rod is changed.

Chapter 6

Conclusions and future work

6.1 Conclusions

From this work, it can be seen that the implementation of an ERT system with voltage excitation is feasible and advantageous. The construction of such a system presents several improvements over the traditional current excitation ERT systems. The lack of a current source simplifies the construction and reduces the system's cost whereas allows an increase on the range of conductivities on the materials to be imaged.

The use of larger electrodes on ERT with voltage excitation reduces considerably the fringe effect, reconstructed images are less distorted and the sensing area is more efficiently constrained into the electrode area. In addition, the ability to image complex conductivity distributions with the very same electrodes and sensing principle used on ECT represents a step further on the integration of a dual modality tomographic system.

The use of driven guards helps to reduce even further the fringe effect on ERT with voltage excitation. Its use can increase considerably the quality of the images obtained with such system due to the farther constraint of the sensing field within the electrode area. In consequence, the obtained images are more reliable and less affected by materials outside the sensing area. In addition, the placement on the outer face of the container's wall make the driven guards inexpensive, easy to build, non -invasive and non-intrusive. However, the use of such guards is restricted to single modality ERT systems. This is because the parasitic capacitance generated in between the external driven guards would increase the standing capacitances, increasing in this way the difficulty of measuring the small changes on inter electrode capacitances due to the change on the permittivity distribution inside the sensing area.

6.2 Future work

On this work it has been shown the advantages of using ERT with voltage excitation and an experimental system has been constructed to test the performance for this approach, this system was built using a Agilent 34972A DAQ and there exists the need for the design of a dedicated data acquisition and control board. It is expected that the use of advanced hardware and signal processing techniques would allow to increase considerably the system's performance.

It has been proved that the use of driven guards for ERT with voltage excitation helps to improve significantly the quality of the reconstructed images. Therefore, there exists the need of further research for the development of more efficient driven guards for a single modality ERT system. Parameters like the guard length or wall width have to be assessed to find the optimum point in which the driven guards could give the maximum advantage to ERT imaging systems.

Due to the sensor's circular geometry, the test grid designed in COMSOL to obtain the sensitivity map does not fit properly inside the region to be tested. It is necessary to design a test grid that suits into the sensor's geometry, allowing in this way to acquire a more accurate sensitivity distribution.

The final goal for future research is the integration of a dual modality tomographic system. The devised system should be capable to image with ECT and ERT modalities simultaneously over an unique set of electrodes. With the aid of signal processing techniques and new hardware design, such system is expected to comply with requirements like a high signal-to-noise ratio (SNR) and an adequate imaging speed.

References

Bhattacharyya P, Mitra A and Purkait P (2013), Design and implementation of an electrical resistance tomography (e.r.t.) system for condition assessment of industrial equipment, *IEEE 1st International Conference on Condition Assessment Techniques in Electrical Systems,* 6-8 December, Kolkata, India, pp. 362-367.

Bian H, Sun J and Yang W (2012), Theoretical analysis method for Howland current source design, *Journal of Measurement Science and Instrumentation*, 3(3), pp. 287-293.

Cao Z, Xu L and Wang H (2009), Image reconstruction technique of electrical capacitance tomography for low-contrast dielectrics using Calderons method, *Measurement Science and Technology*, 20(10), 104027 (12pp)

Cao Z, Xu L, Xu C and Wang H (2010), Electrical resistance tomography(ERT) by using an ECT sensor, *IEEE International Conference on Imaging Systems and Techniques*, 1-2 July, Thessaloniki, Greece, pp. 63-66.

Cui Z, Wang H, Xu Y, Zhang L and Yan Y (2009), An Integrated ECT / ERT Dual Modality Sensor, *IEEE Instrumentation and Measurement Technology Conference*, 5-7 May, Singapore, pp. 1434-1438 .

Dickin F and Wang M (1996), Electrical resistance tomography for process applications, *Measurement Science and Technology*, 7(3), pp. 247-260.

Gamio J C and Martin R (2005), Electrical capacitance tomography two-phase oil-gas pipe flow imaging by the linear back-projection algorithm, *Geofisica internacional,* 44(3), pp. 265-273.

Hao L, Xiang D, Xin D, Shuo T and Yu T (2013), Research on forward problem of tuber electrical resistance tomography system, *IEEE 11th International Conference on Electronic Measurement and Instruments*, 16-19 August, Harbin, China, pp. 197-201.

Harikumar R, Prabu R and Raghavan S (2013), Electrical Impedance Tomography (EIT) and Its Medical Applications : A Review, *International Journal of Soft Computing and Engineering*, 3(4), pp. 193-198.

Khan S H and Abdullah F (1993), Finite element modelling of multielectrode capacitive systems for flow imaging, *IEE Proceedings G Circuits, Devices and Systems,* 140(3), pp. 216-222.

Kim Y S, Lee S H, Ijaz U Z, Kim K Y and Choi B Y (2007), Sensitivity map generation in electrical capacitance tomography using mixed normalization models, *Measurement Science and Technology*, 18(7), pp. 2092-2102.

Kuroda S (1983), A simple stray-free capacitance meter by using an operational amplifier, *IEEE Transactions on Instrumentation and Measurement*, 32(4), pp. 512-513.

Li Y and Yang W (2009), Measurement of multi-phase distribution using an integrated dual-modality sensor, *IEEE International Workshop on Imaging Systems and Techniques*, 11-12 May, Shenzhen, China, pp. 335-339.

Li Y, Yang W, Xie C, Huang S, Wu Z, Tsamakis D, Lenn C (2012), Gas/oil/water flow measurement by electrical capacitance tomography, *Measurement Science and Technology*, 24(7), pp. 112.

Loh W, Waterfall R, Cory J and Lucas G (1999), Using ERT for multi-phase flow monitoring, *1st World Congress on Industrial Process Tomograph*, 14-17 April, Buxton, UK, pp. 4753.

Ma Y, Wang H, Xu L and Jiang C (1997), Simulation study of the electrode array used in an ERT system, *Chemical Engineering Science*, 52(13), July 1997, pp. 2197-2203.

Ma Y, Xu L a and Jiang C (1999), Experimental Study of the Guard Electrodes in an ERT System, *1st World Congress on Industrial Process Tomograph*, 14-17 April, Buxton, UK, pp. 335-338.

Marashdeh Q, Member S, Warsito W, Fan L and Teixeira F (2006), Nonlinear Forward Problem Solution for Electrical Capacitance Tomography Using Feed-Forward Neural Network, *IEEE Sensors Journal,* 6(2), pp. 441-449.

Marashdeh Q and Teixeira F (2004), Sensitivity Matrix Calculation for Fast 3-D Electrical Capacitance Tomography (ECT) of Flow Systems, *IEEE Transactions on Magnetics*, 40(2), pp. 1204-1207.

Marashdeh Q, WarsitoW, Fan L and Teixeira F (2007), A multimodal tomography system based on ECT sensors, *IEEE Sensors Journal*, 7(3), pp. 426-433.

Qiu C, Hoyle B and Podd F (2007), Engineering and application of a dual-modality process tomography system, *Flow Measurement and Instrumentation,* 18(5-6), pp. 247-254.

Styra D and Babout L (2010), Improvement of AC-based electrical capacitance tomography hardware, *Elektronika ir Elektrotechnika*, 7(103), pp. 201-221.

Sun J and Yang W (2012), 3D Effect of Electrical Capacitance and Resistance Tomography Sensors, *IEEE International Conference on Imaging Systems and Techniques,* 16-17 July, Manchester, UK, pp. 562-566.

Sun J and Yang W (2014), Evaluation of fringe effect of electrical resistance tomography sensor, *Measurement: Journal of the International Measurement Confederation*, 18, pp. 145-160.

Sun J and Yang W (2015), A dual-modality electrical tomography sensor for measurement of gas-oil-water stratified flows, *Measurement: Journal of the International Measurement Confederation*, 66, pp. 150-160.

Wang M, Dickin F J and Williams R A (1994), Electrical resistance tomography of metal walled vessels and pipelines. *Electronics Letters,* 30(10), pp. 771-773.

Wang M, Dorward A, Vlaev D and Mann R (1999), Measurements of Gas-Liquid Mixing in a Stirred Vessel Using Electrical Resistance Tomography (ERT), *Chemical Engineering Journal,* 77(1-2), pp. 93-98.

Wang P, Wang H, Sun B, Cui Z and Huang W (2014), An ECT/ERT dual-modality sensor foroil-water two-phase flow measurement *AIP Conference Proceedings,* 13-15 December, Guangzhou, China, pp. 39.

Xie C, Huang S, Beck M, Hoyle B, Thorn R, Lenn C and Snowden D (1992), Electrical capacitance tomography for flow imaging: system model for development of image reconstruction algorithms and design of primary sensors, *IEE Proceedings G Circuits, Devices and Systems*, 139(1), pp. 89-98.

Xu H, Yang G and Wang S (1999), Effect of Axial Guard Electrodes on Sensing Field of Capacitance Tomographic Sensor, *1st World Congress on Industrial Process Tomography,* 14-17 April, Buxton, UK, pp. 348-352.

Yan H, Shao F and Wang S (1999), Simulation Study of Capacitance Tomography Sensors, *1st World Congress on Industrial Process Tomography,* 14-17 April, Buxton, UK, pp. 388-394.

Yang W (1997), Modelling of capacitance tomography sensors, *IEE Proceedings Science, Measurement and Technology,* 144(5), pp. 203-208.

Yang W (2010), Design of electrical capacitance tomography sensors, *Measurement Science and Technology*, 21(4), 042001 (13pp).

Yang W and Conway W F (1998), Measurement of sensitivity distributions of capacitance tomography sensors, *AIP Review of Scientific Instruments*, 69, pp. 233-236

Yang W and Liu S (1999), Electrical Capacitance Tomography with a Square Sensor, *Electronics Letters*, 35(4), pp. 295-296.

Yang W Q and Peng L (2003), Image reconstruction algorithms for electrical capacitance tomography, *Measurement Science and Technology*, 14(1), pp. R1-R13.

Yang W, Spink D M, York T and McCann H (1999), An image-reconstruction algorithm based on Landwebers iteration method for electrical-capacitance tomography, *Measurement Science and Technology*, 10(11), pp. 1065-1069.

Yang W, Stott a L, Beck M S and Xie C (1995), Development of capacitance tomographic imaging systems for oil pipeline measurements, *AIP Review of Scientific Instruments*, 66(8), pp. 4326-4332.

Yenjaichon W, Pageau G, Bhole M, Bennington C P J and Grace J R (2011), Assessment of mixing quality for an industrial pulp mixer using electrical resistance tomography, *The Canadian Journal of Chemical Engineering,* 89(5), pp. 996-1004.

Zhang L (2011), Image reconstruction algorithm for electrical impedance tomography using updated sensitivity matrix, *International Conference of Soft Computing and Pattern Recognition,* 14-16 October, Dalian, China, pp. 248252.

Zhangyong L, Zhui X, Chaoshi R, Wei W, Dechun Z and Huiquan Z (2010), Study of voltage control current source in electrical impedance tomography system, *4th International Conference on Bioinformatics and Biomedical Engineering*, 18-20 June, Chengdu, China, pp. 1-4.

Appendix A

Sensitivity map generation

```
clear all
clc
tic
import com.comsol.model.*
import com.comsol.model.util.*
model = mphload('C:\Users\Marco\Documents\Simulations\ert_non_empty_pixel3.mph');
maps(1:1024,1:28)=0;
x=-3.390625;
y=3.390625;
data(1:1024,1:8)=0;
coord(1,1)=0;
R=1;
r=2;
a=1;


elec_(1,:)=[1578];%
elec_(2,:)=[1574];%
elec_(3,:)=[1568];%
elec_(4,:)=[1564];%
elec_(5,:)=[1563];%
elec_(6,:)=[1567];%
elec_(7,:)=[1573];%
elec_(8,:)=[1577];%



for elec=1:7
    gnd=[];
  for i=1:8
      if i~=elec
          gnd=[gnd elec_(i,:)];
          end
  end
gnd=sort(gnd);
model.physics('ec').feature('gnd1').selection.set([]);
model.physics('ec').feature('pot1').selection.set([]);
model.physics('ec').feature('gnd1').selection.set([gnd]);
model.physics('ec').feature('pot1').selection.set([elec_(elec)]);


all=([1  2  3  4  5  6  7  8  9  10  11  12  13  14  15  16  17  18  19  20  21  22  23  24  25  26  27
    28  29  30  31  32  33  34  35  36  37  38  39  40  41  42  43  44  45  46  47  48  49  50  51  52
    53  54  55  56  57  58  59  60  61  62  63  64  65  66  67  68  69  70  71  72  73  74  75  76  77
    78  79  80  81  82  83  84  85  86  87  88  89  90  91  92  93  94  95  96  97  98  99  100  101
    102  103  104  105  106  107  108  109  110  111  112  113  114  115  116  117  118  119  120
    121  122  123  124  125  126  127  128  129  130  131  132  133  134  135  136  137  138  139
    140  141  142  143  144  145  146  147  148  149  150  151  152  153  154  155  156  157  158
    159  160  161  162  163  164  165  166  167  168  169  170  171  172  173  174  175  176  177
    178  179  180  181  182  183  184  185  186  187  188  189  190  191  192  193  194  195  196
    197  198  199  200  201  202  203  204  205  206  207  208  209  210  211  212  213  214  215
    216  217  218  219  220  221  222  223  224  225  226  227  228  229  230  231  232  233  234
    235  236  237  238  239  240  241  242  243  244  245  246  247  248  249  250  251  252  253
    254  255  256  257  258  259  260  261  262  263  264  265  266  267  268  269  270  271  272
    273  274  275  276  277  278  279  280  281  282  283  284  285  286  287  288  289  290  291
    292  293  294  295  296  297  298  299  300  301  302  303  304  305  306  307  308  309  310
    311  312  313  314  315  316  317  318  319  320  321  322  323  324  325  326  327  328  329
    330  331  332  333  334  335  336  337  338  339  340  341  342  343  344  345  346  347  348
    349  350  351  352  353  354  355  356  357  358  359  360  361  362  363  364  365  366  367
    368  369  370  371  372  373  374  375  376  377  378  379  380  381  382  383  384  385  386
    387  388  389  390  391  392  393  394  395  396  397  398  399  400  401  402  403  404  405
```

```
406 407 408 409 410 411 412 413 414 415 416 417 418 419 420 421 422 423 424
425 426 427 428 429 430 431 432 433 434 435 436 437 438 439 440 441 442 443
444 445 446 447 448 449 450 451 452 453 454 455 456 457 458 459 460 461 462
463 464 465 466 467 468 469 470 471 472 473 474 475 476 477 478 479 480 481
482 483 484 485 486 487 488 489 490 491 492 493 494 495 496 497 498 499 500
501 502 503 504 505 506 507 508 509 510 511 512 513 514 515 516 517 518 519
520 521 522 523 524 525 526 527 528 529 530 531 532 533 534 535 536 537 538
539 540 541 542 543 544 545 546 547 548 549 550 551 552 553 554 555 556 557
558 559 560 561 562 563 564 565 566 567 568 569 570 571 572 573 574 575 576
577 578 579 580 581 582 583 584 585 586 587 588 589 590 591 592 593 594 595
596 597 598 599 600 601 602 603 604 605 606 607 608 609 610 611 612 613 614
615 616 617 618 619 620 621 622 623 624 625 626 627 628 629 630 631 632 633
634 635 636 637 638 639 640 641 642 643 644 645 646 647 648 649 650 651 652
653 654 655 656 657 658 659 660 661 662 663 664 665 666 667 668 669 670 671
672 673 674 675 676 677 678 679 680 681 682 683 684 685 686 687 688 689 690
691 692 693 694 695 696 697 698 699 700 701 702 703 704 705 706 707 708 709
710 711 712 713 714 715 716 717 718 719 720 721 722 723 724 725 726 727 728
729 730 731 732 733 734 735 736 737 738 739 740 741 742 743 744 745 746 747
748 749 750]);


ind=[0,0,0,0,0,0,0,0,0,0,0,0,0,8,7,6,5,4,3,2,0,0,0,0,0,0,0,0,0,0,0,0,0,0,0,0,0,
     0,0,21,20,19,18,17,16,15,14,13,12,11,10,9,0,0,0,0,0,0,0,0,0,0,0,0,0,0,0,0,0,38,
     37,36,35,34,33,32,31,30,29,28,27,26,25,24,23,22,0,0,0,0,0,0,0,0,0,0,0,0,0,0,0,57,
     56,55,54,53,52,51,50,49,48,47,46,45,44,43,42,41,40,39,0,0,0,0,0,0,0,0,0,0,0,0,0,0,
     78,77,76,75,74,73,72,71,70,69,68,67,66,65,64,63,62,61,60,59,58,0,0,0,0,0,0,0,0,0,0,
     0,0,0,101,100,99,98,97,96,95,94,93,92,91,90,89,88,87,86,85,84,83,82,81,80,79,0,0,0,
     0,0,0,0,0,126,125,124,123,122,121,120,119,118,117,116,115,114,113,112,111,110,109,
     108,107,106,105,104,103,102,0,0,0,0,0,0,0,153,152,151,150,149,148,147,146,145,144,143,
     142,141,140,139,138,137,136,135,134,133,132,131,130,129,128,127,0,0,0,0,0,180,179,
     178,177,176,175,174,173,172,171,170,169,168,167,166,165,164,163,162,161,160,159,158,
     157,156,155,154,0,0,0,0,209,208,207,206,205,204,203,202,201,200,199,198,197,196,195,
     194,193,192,191,190,189,188,187,186,185,184,183,182,181,0,0,0,238,237,236,235,234,233,
     232,231,230,229,228,227,226,225,224,223,222,221,220,219,218,217,216,215,214,213,212,211,
     210,0,0,0,267,266,265,264,263,262,261,260,259,258,257,256,255,254,253,252,251,250,249,
     248,247,246,245,244,243,242,241,240,239,0,0,298,297,296,295,294,293,292,291,290,289,288,
     287,286,285,284,283,282,281,280,279,278,277,276,275,274,273,272,271,270,269,268,0,329,328,
     327,326,325,324,323,322,321,320,319,318,317,316,315,314,313,312,311,310,309,308,307,306,
     305,304,303,302,301,300,299,0,360,359,358,357,356,355,354,353,352,351,350,349,348,347,346,
     345,344,343,342,341,340,339,338,337,336,335,334,333,332,331,330,0,391,390,389,388,387,386,
     385,384,383,382,381,380,379,378,377,376,375,374,373,372,371,370,369,368,367,366,365,364,
     363,362,361,0,422,421,420,419,418,417,416,415,414,413,412,411,410,409,408,407,406,405,
     404,403,402,401,400,399,398,397,396,395,394,393,392,0,453,452,451,450,449,448,447,446,
     445,444,443,442,441,440,439,438,437,436,435,434,433,432,431,430,429,428,427,426,425,424,
     423,0,484,483,482,481,480,479,478,477,476,475,474,473,472,471,470,469,468,467,466,465,
     464,463,462,461,460,459,458,457,456,455,454,0,0,513,512,511,510,509,508,507,506,505,504,
     503,502,501,500,499,498,497,496,495,494,493,492,491,490,489,488,487,486,485,0,0,0,542,
     541,540,539,538,537,536,535,534,533,532,531,530,529,528,527,526,525,524,523,522,521,520,
     519,518,517,516,515,514,0,0,0,571,570,569,568,567,566,565,564,563,562,561,560,559,558,
     557,556,555,554,553,552,551,550,549,548,547,546,545,544,543,0,0,0,0,598,597,596,595,594,
     593,592,591,590,589,588,587,586,585,584,583,582,581,580,579,578,577,576,575,574,573,572,
     0,0,0,0,0,625,624,623,622,621,620,619,618,617,616,615,614,613,612,611,610,609,608,607,
     606,605,604,603,602,601,600,599,0,0,0,0,0,0,650,649,648,647,646,645,644,643,642,641,640,
     639,638,637,636,635,634,633,632,631,630,629,628,627,626,0,0,0,0,0,0,0,0,673,672,671,670,
     669,668,667,666,665,664,663,662,661,660,659,658,657,656,655,654,653,652,651,0,0,0,0,0,0,
     0,0,0,0,694,693,692,691,690,689,688,687,686,685,684,683,682,681,680,679,678,677,676,675,
     674,0,0,0,0,0,0,0,0,0,0,0,0,713,712,711,710,709,708,707,706,705,704,703,702,701,700,699,
     698,697,696,695,0,0,0,0,0,0,0,0,0,0,0,0,0,0,730,729,728,727,726,725,724,723,722,721,720,
     719,718,717,716,715,714,0,0,0,0,0,0,0,0,0,0,0,0,0,0,743,742,741,740,739,738,737,
     736,735,734,733,732,731,0,0,0,0,0,0,0,0,0,0,0,0,0,0,0,0,0,0,0,750,749,748,747,746,
     745,744,0,0,0,0,0,0,0,0,0,0,0,0,0,0,0,0,0,0,0,0,0,0,0,0,0,0,0,0,0,0,0,0,0,0,0,0,0,0,0];

 elec
 data(1,1)=0;
 R=1;

for x=1:1024
    if ind(x)~=0

        Y=[ind(1:x−1) ind(x+1:1024)];
        y=find(Y~=0);
        G=Y(y);
        G=sort(G);
model.material('mat8').selection.set([1 G]);
model.material('mat6').selection.set([ ind(x)]);


model.study('std1').run    %run the study
model.result('pg1').run;
model.result.numerical('int1').appendResult; %get the integral value and save it on the table
model.result.numerical('int2').appendResult;
model.result.numerical('int3').appendResult;
model.result.numerical('int4').appendResult;
model.result.numerical('int5').appendResult;
model.result.numerical('int6').appendResult;
model.result.numerical('int7').appendResult;
model.result.numerical('int8').appendResult;
```

```
     str1=mphtable(model,'tbl1'); %recover the value of the integrals on the table
        data(R,1)=str1.data(r+1);
        str1.data(r+1)

        str2=mphtable(model,'tbl2'); %recover the value of the integrals on the table
        data(R,2)=str2.data(r+1);
        str2.data(r+1)

        str3=mphtable(model,'tbl3'); %recover the value of the integrals on the table
        data(R,3)=str3.data(r+1);
        str3.data(r+1)

        str4=mphtable(model,'tbl4'); %recover the value of the integrals on the table
        data(R,4)=str4.data(r+1);
        str4.data(r+1)

        str5=mphtable(model,'tbl5'); %recover the value of the integrals on the table
        data(R,5)=str5.data(r+1);
        str5.data(r+1)

        str6=mphtable(model,'tbl6'); %recover the value of the integrals on the table
        data(R,6)=str6.data(r+1);
        str6.data(r+1)

        str7=mphtable(model,'tbl7'); %recover the value of the integrals on the table
        data(R,7)=str7.data(r+1);
        str7.data(r+1)

        str8=mphtable(model,'tbl8'); %recover the value of the integrals on the table
        data(R,8)=str8.data(r+1);
        str8.data(r+1)

        r=r+1
        R=R+1
    else
        data(R,1)=0; %value of the current with the sensor full of water
        data(R,2)=0;
        data(R,3)=0;
        data(R,4)=0;
        data(R,5)=0;
        data(R,6)=0;
        data(R,7)=0;
        data(R,8)=0;
        R=R+1
end

end
  for indx=elec+1:8

      maps(:,a)=data(:,indx);
      a=a+1;
  end

end
toc
```

Appendix B

Sensitivity map generation dot product

```
%calculate the sensitivity matrix
function [Sensitivity_Matrix]=Sensitivity8elecERT()

%clear all;clc;
size=32;
E_No = 8;
S_No = 7;

for i=1:E_No

    p = load(strcat('C:\Users\Marco\Documents\Simulations\sens ERT\32_32\32_32 adjoint method\data',num2str(i),'.txt'));

        p = real(p(:,3));
        ind = find(isnan(p));p(ind) = 0;
        pot1(:,i) = p;
end

% Set Region of interest (RoI) values to 1, others to 0
RoI=load('C:\Users\Marco\Documents\Simulations\sens ERT\32_32\32_32 adjoint method\image area.txt');
RoI=RoI(:,3); % Exported from COMSOL
idx = find(RoI==[9.40000000000000e-05;]);
RoI=zeros(length(RoI),1);
RoI(idx)=1;
RoI=reshape(RoI,size*size,1);

% sensitivity matric for independent measurement
Element_Line=0;
for i=1:S_No
        % Calculate eletric field from potential data
        for j=1:(E_No)%-i)
            e1=pot1(:,i);
            e1=reshape(e1,size,size);
            [ex,ey]=gradient(e1);
            e1_x=reshape(ex,size*size,1);
            e1_y=reshape(ey,size*size,1);

            e2=pot1(:,i+j);
            e2=reshape(e2,size,size);
            [px,py]=gradient(e2);
            e2_x=reshape(px,size*size,1);
            e2_y=reshape(py,size*size,1);

            A=e1_x.*e2_x;
            B=e1_y.*e2_y;

            s=(-1)*(A+B);
            s=s.*RoI;
            Element_Line=Element_Line+1;
            s1(:,Element_Line)=s;
        end
end
Sensitivity_Matrix=s1;
%End
```

Appendix C

Image Reconstruction

```
clc
clear all
n_elec=8;    %number of electrodes

SIZE=32;     %size of reconstructed image

sc=Sensitivity8elecERT(); % function call to obtain the sensitivity matrix
load('C:\Users\Marco\Documents\Simulations\sens ERT\32_32\32_32 test un solo mph\maps_norm_best');
sc1=maps_norm;


n_iter=050;    %number of iterations, 0 LBP more than 0 Landweber
kp=1.2;        %Relaxation factor



load('C:\Users\Marco\Google Drive\off\10k\rod1.txt')
c_m=rod1;%measurements.data(:,2);% rod8;%(:,4);%



load('C:\Users\Marco\Google Drive\off\10k\low.txt')
c_l=low;


load('C:\Users\Marco\Google Drive\off\10k\meas_hi.txt')
c_h=meas_hi;%measurements.data(:,2);% meas_hi8%(:,4);%



n_meas=(n_elec*(n_elec-1))/2;  %number of independant measurements n=m(m-1)/2; n = number of measurements, m=number of electrodes

for i=1:n_meas    %normalization of measurements norm=(c_m-c_l)/(c_h-c_l)
    norm(i)=(c_m(i)-c_l(i))./(c_h(i)-c_l(i));
end


sc_t=sum(sc,2);
sm=sc';
img=norm*sm;
img=img';

ind=find(sc_t==0);
sc_t(ind)=1;
img=img./sc_t;


for i=1:n_iter
    im=img';
    a=im*sc;
    a=norm-a;
    a=sc*a';
    %kp=kp+.0000001;
    img=img+kp*a;

end
kp
for nn=1:SIZE*SIZE
    if img(nn)<0 img(nn)=0;end
    if img(nn)>1 img(nn)=1;end
end
```
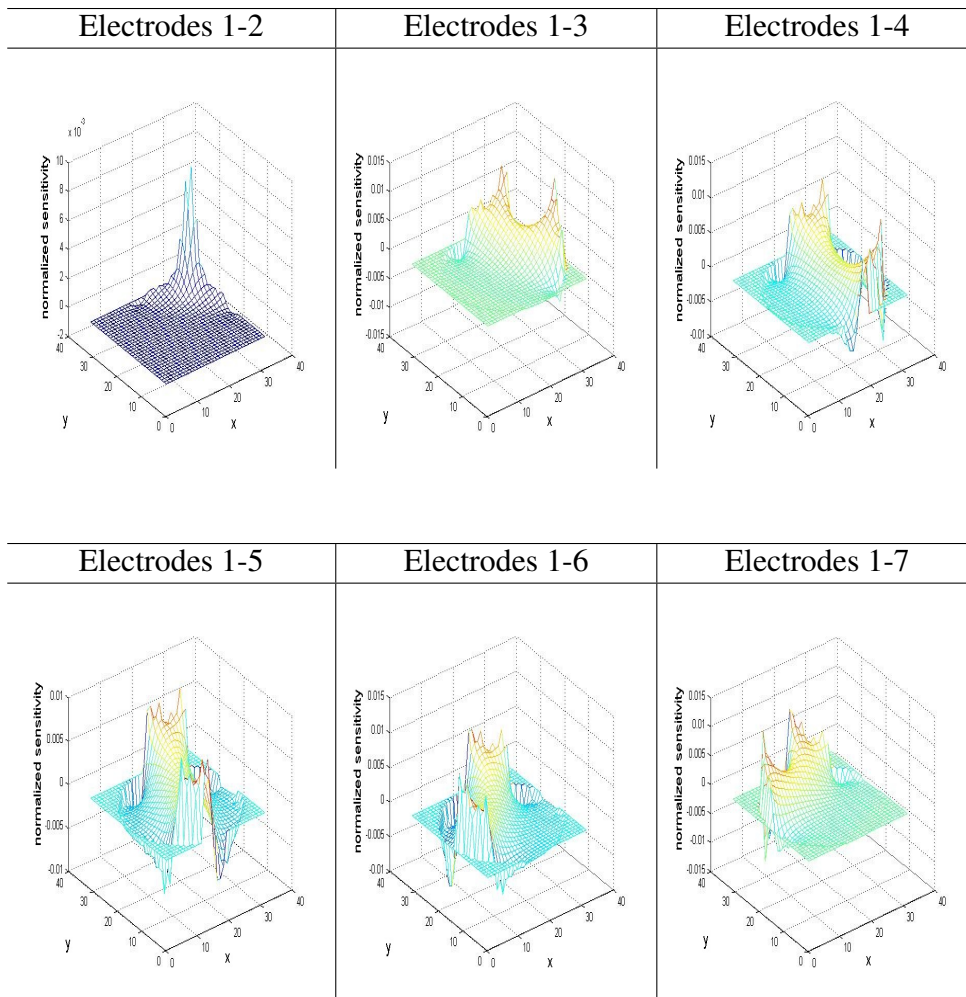
```
figure;
cc=reshape(img*1,SIZE,SIZE);
surface(cc);
daspect([1,1,1]);

colorbar;
axis off;
shading flat;
```
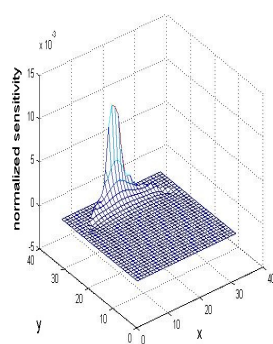
Appendix D

Sensitivity map COMSOL CAD

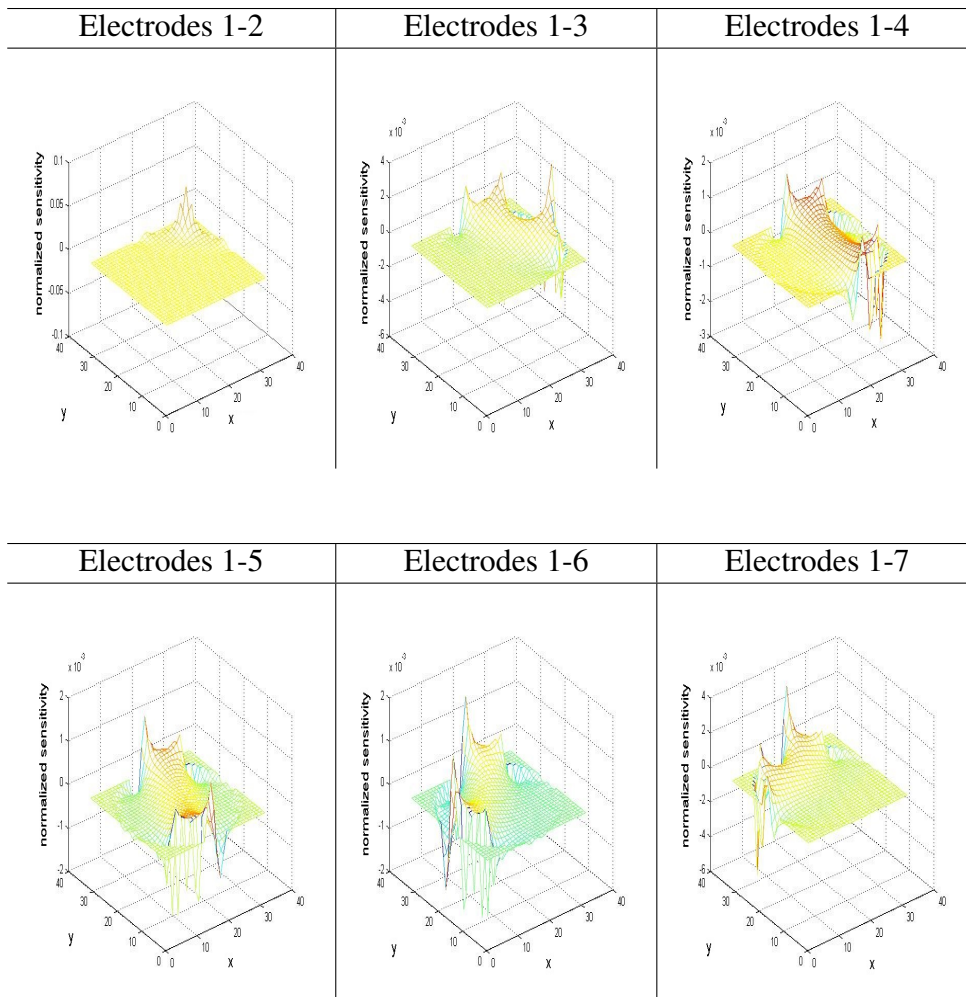| Electrodes 1-2	Electrodes 1-3	Electrodes 1-4

Electrodes 1-5	Electrodes 1-6	Electrodes 1-7

Electrodes 1-8

Appendix E

Sensitivity map electric fields

Electrodes 1-2	Electrodes 1-3	Electrodes 1-4
Electrodes 1-5	Electrodes 1-6	Electrodes 1-7

Electrodes 1-8